SLAC DIVERTOR CHANNEL ENTRANCE THERMAL STRESS ANALYSIS

Gary L. Johnson
Werner Stein
Stephen C. Lu
Robert A. Riddle

July 10, 1985

Lawrence Livermore National Laboratory

DISCLAIMER

Page Range	Domestic Price	Page Range	Domestic Price
001-025	$ 7.00	326-350	$ 26.50
026-050	8.50	351-375	28.00
051-075	10.00	376-400	29.50
076-100	11.50	401-426	31.00
101-125	13.00	427-450	32.50
126-150	14.50	451-475	34.00
151-175	16.00	476-500	35.50
176-200	17.50	501-525	37.00
201-225	19.00	526-550	38.50
226-250	20.50	551-575	40.00
251-275	22.00	576-600	41.50
276-300	23.50	601-up[1]	
301-325	25.00		

[1]Add 1.50 for each additional 25 page increment, or portion thereof from 601 pages up.

TABLE OF CONTENTS

LIST OF TABLES

Page

LIST OF FIGURES

Page

ABSTRACT

X-ray beams emerging from the new SLAC electron-positron
storage ring (PEP) impinge on the entrance to tangential
divertor channels causing highly localized heating in the
channel structure. Analyses were completed to determine the
temperatures and thermally-induced stresses due to this
heating. These parts are cooled with water flowing axially
over them at 30 $^{\circ}$C. The current design and operating
conditions should result in the entrance to the new divertor
channel operating at a peak temperature of 123 $^{\circ}$C with a peak
thermal stress at 91% of yield. Any micro-cracks that form
due to thermally-induced stresses should not propagate to the
coolant wall nor form a path for the coolant to leak into the
storage ring vacuum.

SUMMARY

X-ray beams emerging from the new SLAC electron-positron storage ring (PEP) can impinge on the entrance to tangential divertor channels. This causes highly localized heating and thus highly localized thermal stresses in the channel structure. Shifting the beam orientation can cause a corresponding shift in this locally heated and stressed region.

The resultant temperatures and thermally-induced stresses in the divertor entrance were determined using the LLNL finite element heat transfer computer code TACO3D and the LLNL finite element structural computer code GEMINI. The geometry of the 6061-T6 aluminum structure is described in Figure 1. Room temperature thermal/mechanical properties are used for the 6061-T6 aluminum. The nose and the length of the 7.5° ramped surface of the divertor absorb the x-ray beam for all but one case. The x-ray beam originating from the undulator falls only on a portion of the ramp. The absorbed x-rays are modeled as a "local heat generation". All surfaces are assumed to be adiabatic except the outside surfaces of the walls parallel to the plane of symmetry. Water flows axially over these surfaces at $30\ ^{\circ}C$. All surfaces are assumed to be structurally free (unloaded and able to move in any direction) except the centerplane and the front/rear planes which have zero displacement limits.

For the design case, peak temperatures are lowest when the convective heat transfer coefficient is greater than $1.5\ W/cm^2\ K$. The temperature gradients are especially high within 2 mm to 5 mm of the location of the highest temperature. The high thermal conductivity of the aluminum does, however, reduce the temperature gradients substantially

thereafter. Using the most probable heat transfer
coefficient (i.e. 1.9 W/cm^2), the peak temperature is near
the minimum (123 $^{\circ}$C) for nose heights greater than 6 mm. A
decrease of 7 $^{\circ}$C in the peak temperature (compared to that
for the centered beam) occurs when the bending magnet mis-
steers the beam to the side wall. When the x-ray beam
originates in the undulator, the peak temperature is 101 $^{\circ}$C.

For the design case, the peak thermally-induced stress stays
below the yield stress at heat transfer coefficients above
1.0 W/cm^2 K. The yield stress for the aluminum is defined at
the local element temperature. The stresses in all analyses
are well below yield within 2 mm to 3 mm of the peak stress
location. Using the most probable heat transfer coefficient,
the peak stress is below yield for minimum nose heights
greater than 4 mm. The peak thermal stress for the mis-
steered bending magnet beam case is about 56 MPa greater than
when the beam is centered. For the undulator source beam,
the peak stress is 53.4% of yield stress.

A fracture mechanics study shows that

    (a) micro-cracks will probably form in those regions
    where the stress greater than the yield stress,

    and
    (b) these cracks will not propagate to the wall since
    the temperatures and thermally-induced stresses are much
    lower a short distance from the locations of the peak
    conditions.

The current design and operating conditions should result in
the structure of the channel running at a peak temperature of
123 $^{\circ}$C with a peak thermal stress of 91% of yield. Any
cracks that form should not propagate to the coolant wall
forming a path for water leaks into the storage ring vacuum.

INTRODUCTION

X-ray beams can emerge from the new SLAC electron-positron storage ring (PEP) into tangential side channels (divertors) connecting with experimental chambers. These beams result from the bending of the electron-positron streams by the ring's bending magnets or from repeated bending in the ring's undulator section (used to generate a directed, intense x-ray beam). One tangential channel near the undulator exits the ring to an x-ray beam test facility. The entrance of this channel has a tapered transition section (or crotch) of 6061-T6 aluminum between the storage ring wall and the channel wall.

The beams impinge on the crotch causing highly localized heating (Figure 1.). This heating can vary in location because of shifts in the magnetic fields of the bending magnets or the undulator. Highly localized heating in a constrained structure will induce large local thermal stresses. Inhibiting the axial motion of the channel model's end planes structurally constrains the divertor section.

Thermally-induced stresses in elastic media are modeled with the term $- a E \, \Delta T/(1-2\upsilon)$ added to the general stress-strain expressions for the normal stresses. In this term a is the coefficient of thermal expansion, E is the elastic modulus, υ is Poisson's ratio, and ΔT is the temperature change from the stress-free condition reference state.

The analytical model simulates the absorption of the x-ray beams in a volume of the aluminum channel structure by imposing a corresponding "local heat generation" in the same region. The absorption rate is based on 1-D absorption calculations by Stanford.

Analyses were completed to determine the resultant
temperatures and thermally-induced stresses in the divertor
entrance for several beam orientations and entrance designs.
The temperature distributions are calculated based on a three
dimensional, steady state, linear heat transfer analysis
using the LLNL finite element computer code, TACO3D. The
calculated temperatures were used as input for the three
dimensional, steady state, linear stress analyses using the
LLNL finite element computer code GEMINI to determine the
thermally-induced stresses.

DISCUSSION

Channel Geometry

The divertor entrance is a ramped, rectangular channel
(Figure 1a). Where the heating is symmetric relative to the
centerplane, only half of it is modeled as shown in Figure
1b. For the asymmetric heating analysis, the entire cross
section is modeled. All length and radius dimensions are in
mm. The figure has the part rotated 90° about the z axis
from its actual orientation on the ring.

The ramp makes an angle of 7.5° with the yz plane of the
model. The nose is perpendicular to the yz plane. Most of
the nose is at a 45° angle to the top (and bottom) walls.
Near the centerplane, the nose is filleted to a 3 mm radius.
No other inside fillets are modeled because of the difficulty
in zoning the fillets. The minimum nose height for each case
is given in Table I. The model outlines for the five cases
are shown schematically in Figures 2 through 6.

Model Boundary Conditions

The thermal boundary conditions are summarized in Table I and
Figures 7 through 11. All surfaces are assumed to be
adiabatic (no energy flow across the surface) with the
exception of the flat outside surface of the top (and bottom)
walls parallel to the centerplane and those along the beam
path. There are twelve 0.13 cm by 0.51 cm axial fins on the
convectively cooled surface resulting in a 400% increase in
surface area over flat walls. For easy analysis, the fins
were not modeled as finite elements, but their influence is
carried in a scaled up heat transfer coefficient on this
interface. The coefficient is scaled based on the area ratio
between the model's cooled wall and the actual part's cooled
wall. We did not include the increased resistance due to the
fins finite thermal conductivity; however, this is not a bad
model since aluminum has such good conductivity.

On this outside surface the convective heat transfer boundary
condition is due to the axial flow of 30 ^{o}C water. Three
cases were completed in the initial analyses on the base case
geometry (i.e. min. nose height=11.71 mm): (a) Case 1A-
convection heat transfer coefficient, h, = 3.8 watts/cm^2 K
(typical of nucleate boiling conditions in water),
(b) Case 1B-h = 0.38 watts/cm^2 K (typical of single phase
water flow conditions), and (c) Case 1D-h = 1.9 W/cm^2 K
(representing single phase water flow scaled from (b) for the
five fold heat transfer area ratio between the flat and
finned walls). For the rest of the cases, the scaled, single
phase heat transfer coefficient (1.9 W/cm^2 K) was employed.

The structural boundary conditions are described in Figures
12 through 16. All surfaces are assumed to be free (unloaded
and able to move in any direction) with the exception of the
centerplane and the front/rear planes. The front/rear planes

have their allowable displacement in the "z" direction set to zero. For all but Case 3, the centerplane has its allowable displacement in the "y" direction set to zero. For Case 3, the outside surface of the wall farthest from the beam has its allowable "y" displacement set to zero. The node on the corner of the x=0 plane, the rear plane, and the "no y displacement" plane has its allowable "x" displacement set to zero.

There are no pressure loads applied to the convectively cooled walls due to coolant pressure because the hydrostatic pressure (about 200 psi) is significantly lower than the expected thermal stresses (on the order of 20 kpsi to 40 kpsi).

Heat Loads

The absorbed energy heat load from the x-ray beam is modeled as a "local heat generation". For all but one case (Case 3), the x-ray beam is absorbed into the nose of the divertor crotch and into the full length of its 7.5° ramped surface (Figures 7 through 11). For Case 3 (modeling the thermal loading from the x-ray beam originating in the undulator) the beam, 5.2 mm tall and centered at 16.93 mm from the yz plane, falls on the ramped portion of the crotch. Each beam is assumed to be uniform over its 0.6 mm width (or 0.3 mm width for the symmetric models).

The x-ray energy deposition rate and its corresponding local heat generation rate are given in Tables II and III. The tables give the total power absorbed (per unit width in the "x" direction) from the full width beam up to a given penetration depth (in the "z" direction). The "local heat generation rate" is determined by calculating the rate of change of absorbed power with depth, then dividing by the x-ray beam width (in the "y" direction). Table II gives the

--14--

heat load based on bending magnet source x-ray beams (i.e., all but Case 3), and Table III gives the heat load based on the undulator source x-ray beam (i.e., Case 3).

Material Properties

The divertor entrance is made of 6061-T6 aluminum. The analyses used the following room temperature thermal and mechanical properties for this material (derived from the references - Metals' Handbook, 8th edition and the Structural Alloy Handbook, 1973).

density	= 2710 kg/m^3
specific heat	= 963 (W s)/kg K
conductivity	= 166.15 W/m K
thermal expansion coefficient	= 2.369 x 10-5 m/m K
elastic modulus	= 68,900 MPa (10100 kpsi)
Poisson's ratio	= 0.3
yield strength	= 283 MPa (41.6 kpsi)

The thermal properties of 6061-T6 aluminum do not change significantly over the expected temperature range 0 $^\circ$C to 150 $^\circ$C. The elastic modulus decreases with increasing temperature, while the coefficient of thermal expansion increases with temperature (Figure 17). The product of these two properties decreases slightly with temperature. Since the thermal stresses are proportional to the product of the elastic modulus and the thermal expansion coefficient, the predicted thermal stresses based on temperature dependent properties would be slightly lower than those predicted based on room temperature properties. The yield stress decreases with increasing temperature, especially the annealing temperature of 120 $^\circ$C where T6 aluminum changes to T4.

Finite Element Zoning

The zoning of the parts for the finite element analyses used the SLIC computer code (a 2-D and 3-D finite element mesh generator) developed at LLNL. Table I gives the number of nodes and elements for each case. Variable spacing between nodes was used to concentrate nodes in areas of high thermal gradients (and, thus high thermal-stress levels). The high gradients were expected near the interfaces between the hot volumes absorbing the x-rays and the unheated adjacent volumes (Figures 7 through 11). The same zoning was used for both the TACO3D heat transfer calculations and the GEMINI stress calculations. A schematic of the zoning for the first analyses is shown in Figure 18. Schematics of each zoning are included in Appendix A.

RESULTS

Thermal Analyses

A summary of the results of the analyses is documented in Table IV and Figures 19 through 34. More detailed results in the form of zoning schematics, isotherm plots, and isobar plots are included in Appendix A. The channel design has a mininum nose height equal to 11.71 mm. The results of the heat transfer calculations for this geometry (Cases 1A, 1B, and 1D) show that a convective heat transfer coefficient greater than 1.5 W/cm^2 K limits the peak temperature to about 125 $^\circ$C (Figure 19).

The peak temperature occurs near the x=0 plane on the intersection of the y=0 and z=0 planes. The peak temperature remains above 120 $^\circ$C at all but the highest h checked. A review of the isotherm plots (Figures 21 through 23 and

Appendix A) shows that the temperature gradients are especially high within 6 to 9 beam half-widths (about 2 mm to 5 mm) of the location of the peak temperature. The high thermal conductivity of the aluminum substantially lowers the temperatures outside this region.

The heat transfer calculation for the case of the mis-steered beam generated in the bending magnet (Case 2) results in a peak temperature about 7 ^{o}C lower than the calculation for the centered beam (Case 1D). (Figure 19 and Figure 24.) This lower temperature is accompanied by a much larger temperature gradient in the top wall.

The heat transfer calculation for the case of the x-ray beam originating in the undulator (Case 3) gives a peak temperature of 101 ^{o}C. (See Figures 19 and 25.) The corresponding temperature gradients are much lower than in the calculation for the heating due to the bending magnet beam.

The entrance can see a heat load resulting from a combination of both the bending magnet beam and the undulator beam. The peak temperature was estimated by adding the difference between the peak temperature and the coolant temperature for the undulator-beam-only calculation to the peak temperature for the bending magnet-beam-only calculation. This gives a worst case peak temperature of 140 ^{o}C. This is probably very conservative since the high aluminum thermal conductivity would redistribute the heat from the added load and moderate the peak temperature. We expect that the actual peak temperature for the design operation conditions will be closer to 125 ^{o}C for the combined beam.

Cases 1D, 4, and 5 check the effect of channel entrance nose height for a heat transfer coefficient, h, equal to 1.9 W/cm^{2} K. The results of these heat transfer calculations

show that the peak temperature remains near the minimum
(123 $^{\circ}$C) for nose heights greater than 6 mm (Figures 20, 23,
26, and 27). Below this height, the peak temperature rises
very rapidly. This probably occurs because the area in the
nose available for heat transfer to the cooled wall is small.

Stress Analyses

For the analyses of the divertor design geometry (i.e. where
minimum nose height = 11.71 mm), the peak stress stays below
the yield stress for heat transfer coefficients above
1.0 W/cm^2. (See Figure 19.) The yield stress is defined by
the local element temperature. Extrapolating from the
figure, the peak stress would seem never to drop below 88% of
yield for any reasonable coolant flowrate at 30 $^{\circ}$C.

A lower peak temperature would improve this situation in two
ways:

    (a) a lower peak temperature with the same coolant
    temperature means smaller temperature gradients and
    corresponding smaller thermal stresses; also

    (b) a lower peak temperature means the limiting yield
    stress of the material is higher giving more margin.

Two possible ways for lowering the thermal stress level
further are:

    (a) lower the coolant temperature (thus lowering the
    peak temperature while maintaining the same temperature
    gradients), or

    (b) raise the effective thermal conductivity of the
    aluminum near the nose of the peak temperature location
    (thus lowering both the peak tempeature and the local
    temperature gradient).

The peak stress occurs just outside the volume heated by the
x-ray beam and below the nose surface. The high stresses are

concentrated in a small volume of the nose. They are well below yield within 6 to 9 beam half-widths (2 mm to 3 mm) of the peak stress location. (See Figures 28 through 30.) Thus, any failure due to yield should be limited to a small region near the irradiated portion of the nose.

The peak thermal stress for the mis-steered beam (Case 2) is about 56 MPa (i.e. 18% of yield) higher than the stress for the centered bending magnet beam case. (See Figures 19 and 31). Although the part is cooler, the large temperature gradient, resulting from the nearby coolant stream, causes higher thermally-induced stresses. The peak stress seems to occur inside the wall rather than on its surface. Since the wall fillets provided in the design for stress relief were not modeled, these calculated stresses are conservative.

The thermal stress calculation for the case of the x-ray beam originating in the undulator (Case 3) gives a peak stress of 141 MPa (or 53.4% of yield stress). (See Figures 19 and 32.) A reliable prediction for the peak thermally-induced stress due to combined heat loads can't be estimated by linear addition of the predicted stresses of the two individual components. Intuitively, based on the expected peak temperature for this situation, the combined load beam peak stress should be about equal to the peak stress calculated for the bending magnet beam.

For the analyses studying the effect of nose height (Cases 1D, 4, and 5), the peak stress remains below yield for minimum nose heights greater than 4 mm. (See Figures 20, 30, 33, and 34.) Below this height the peak stress rises sharply, probably as a result of the large increase in the peak temperature and its associated larger temperature gradient.

Fracture Mechanics

Since the part under some boundary conditions and heat loads
can experience plastic deformation each time the beams are
deflected into the divertor channel, we were asked to
complete a cursory analysis of the possibility of cracks
forming in the peak stress region and propagating to the
water-cooled wall. The results of this analysis are
documented in Appendix B.

The general conclusions of the analysis are
      (a) micro-cracks will probably form in those regions
      which experience stress greater than the yield stress
      and
      (b) these cracks will not propagate to the wall since
      the temperatures and thermally-induced stresses decrease
      sharply in the direction of the water-cooled wall.

CONCLUSIONS

The current design and operating conditions should result in
the crotch running at a peak temperature of 123 °C with a
peak thermal stress of 91% of yield. Any cracks that do form
will not propagate to the wall since the temperatures and
thermally-induced stresses are much lower a short distance
from the locations of the peak conditions.

The peak temperature and the peak stress can be easily
lowered by reducing the coolant temperature to at least 15
°C. This will keep the material below the Al 6061 T6 to
Al 6061 T4 transition temperature with its associated
decrease in yield stress. With this coolant temperature, the
peak stress could be reduced to about 85% of yield.

Table I

Analyses Cases Synopsis

Case No.	X-ray Beam Source	Location of Heating	Beam Height/Width (mm)	Minimum Nose Height (mm)	Heat Transfer Coefficient* (W/cm^2)	Number of Nodes	Number of Elements
1A	Bend. Mag.	Centerplane	32/0.3	11.71	3.8	5498	4236
1B	Bend. Mag.	Centerplane	32/0.3	11.71	0.38	5498	4236
1D	Bend. Mag.	Centerplane	32/0.3	11.71	1.9	5498	4236
2	Bend. Mag.	Next-to-Wall	32/0.6	11.71	1.9	3182	2376
3	Undulator	Centerplane	5.2/0.3	11.71	1.9	4002	3042
4	Bend. Mag.	Centerplane	32/0.3	1.00	1.9	5498	4236
5	Bend. Mag.	Centerplane	32/0.3	6.00	1.9	5498	4236

* For water at $30^{o}C$

Table II
Heat Generation from the X-Ray Beam Originating in the Bending Magnet

Depth (cm)	Total Power Absorbed (Watts/cm)	Heat Generation Rate (W/cm^3)
0.000	0.00	1.79×10^5
0.002	21.52	1.20×10^5
0.004	28.696	5.06×10^4
0.006	33.673	3.73×10^4
0.008	37.636	3.05×10^4
0.01	40.988	2.41×10^4
0.015	47.77	2.03×10^4
0.02	53.18	1.56×10^4
0.03	61.757	1.29×10^4
0.04	68.602	9.84×10^3
0.06	79.476	8.16×10^3
0.08	88.182	6.71×10^3
0.1	95.57	5.34×10^3
0.15	110.58	4.50×10^3
0.2	122.57	3.44×10^3
0.3	141.52	2.82×10^3
0.4	156.44	2.27×10^3
0.5	168.8	1.91×10^3
0.6	179.37	1.65×10^3
0.7	188.58	1.45×10^3
0.8	196.71	1.28×10^3
0.9	203.97	1.15×10^3
1.0	210.51	1.04×10^3
2.0	252.26	406.
3.0	272.76	248.
4.0	284.09	142.
5.0	290.71	85.
6.0	294.73	53.

Table III
Heat Generation from an X-Ray Beam Originating in the Undulator

Depth (cm)	Heat Generation Rate (W/cm^3)
0.000	1.92×10^5
.002	1.44×10^5
.004	8.56×10^4
.006	6.91×10^4
.008	5.94×10^4
.01	4.89×10^4
.015	4.20×10^4
.02	3.28×10^4
.03	2.73×10^4
.04	2.11×10^4
.06	1.75×10^4
.08	1.43×10^4
.1	1.11×10^4
.15	9.08×10^3
.2	6.43×10^3
.3	4.93×10^3
.4	3.67×10^3
.5	2.90×10^3
.6	2.38×10^3
.7	2.01×10^3
.8	1.73×10^3
.9	1.51×10^3
1.	1.33×10^3
2.	515.
3.	250.
4.	133.
5.	75.
6.	45.

Table IV
Analysis Results Synopsis

Case No.	Maximum Temperature (°C)	Location of Max. T (Node No.)	Maximum Stress (MPa)	Location of Max. Stress (Elem No.)	Maximum Stress* (%of Yield)
1A	119.	6	228.	312	89.7
1B	147.	1	279.	616	125.7
1D	123.	6	234.	312	91.0
2	116.	1287	290.	258	109.0
3	101.	280	141.	78	53.4
4	130.	1	311.	312	128.0
5	123.	6	244.	312	97.2

* Versus tensile yield at the temperature of the maximum stress element.

a) Model Outline

b) Half Section
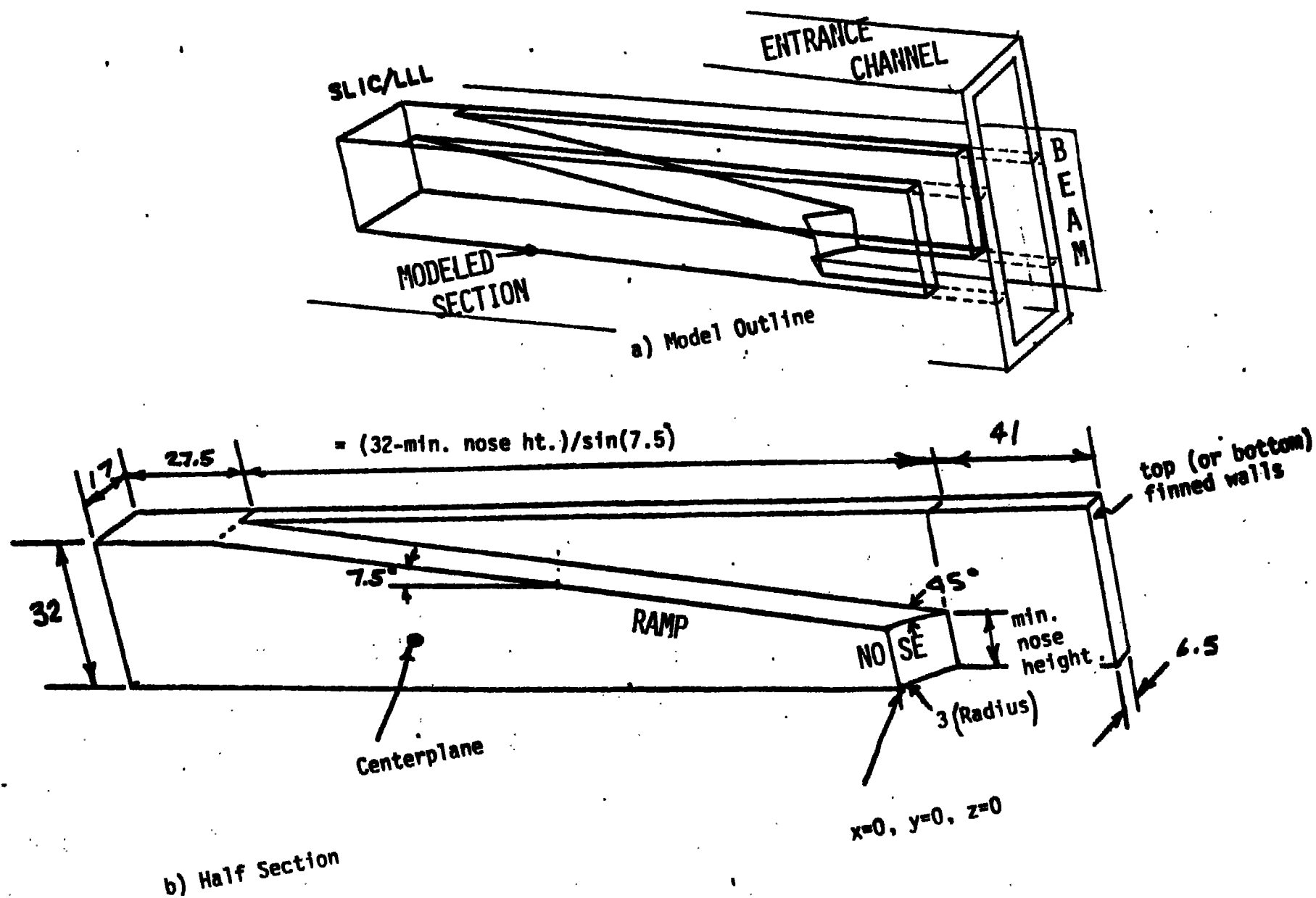
Figure 1. Schematic of the divertor channel entrance with the characteristic dimensions in mm.

OUTLINE OF EDGES

CASE NO. 1 – BASE CASE WITH VARIABLE H

$H = 3.8, \ .38, \ 1.9 \ W/CM^2$

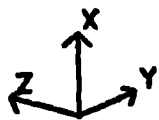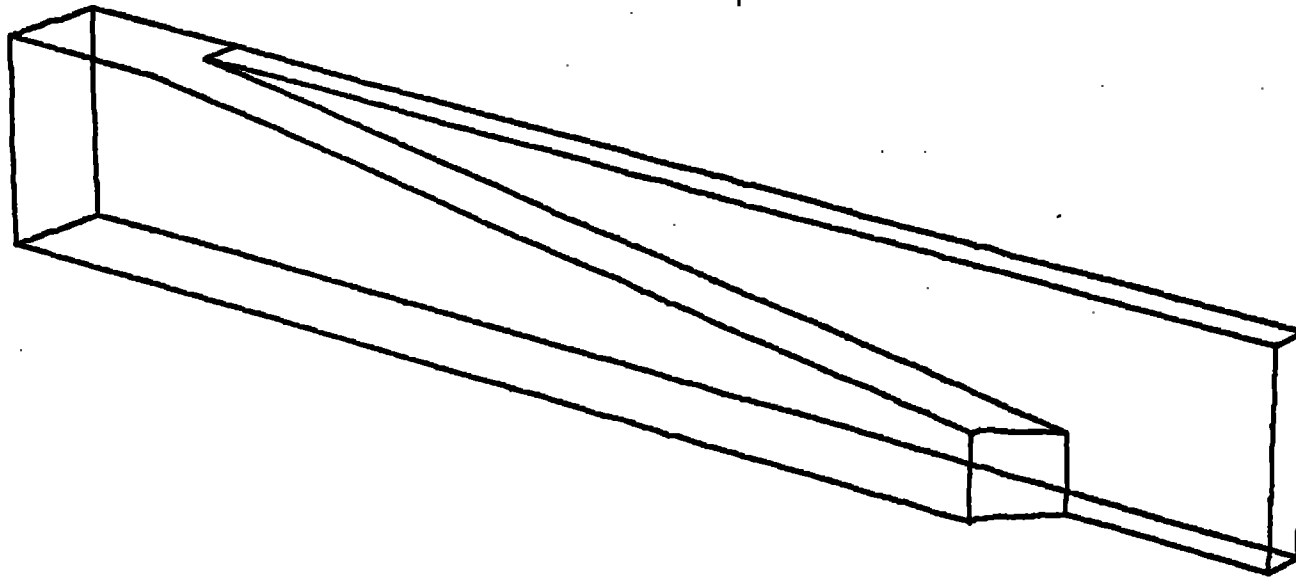MIN. NOSE HEIGHT = 11.71 MM
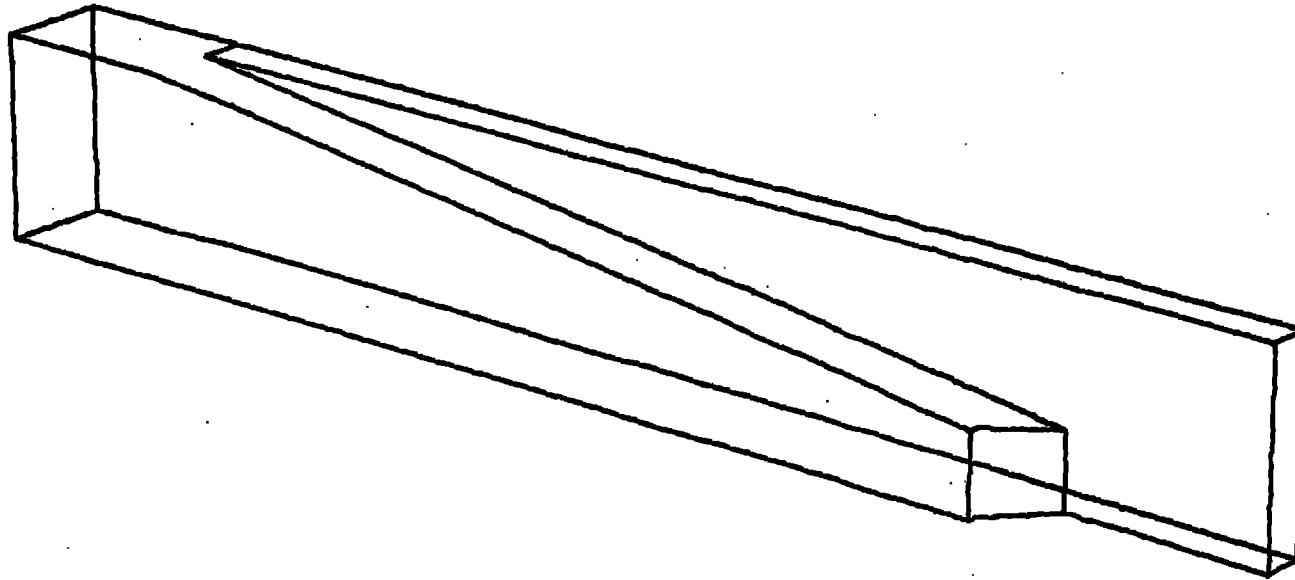
Figure 2. Schematic outline of the modeled part for the base geometry case (#1) studying the effect of the heat transfer coefficient.

OUTLINE OF EDGES

CASE NO.2 — BENDING MAGNET BEAM OFFSTEER

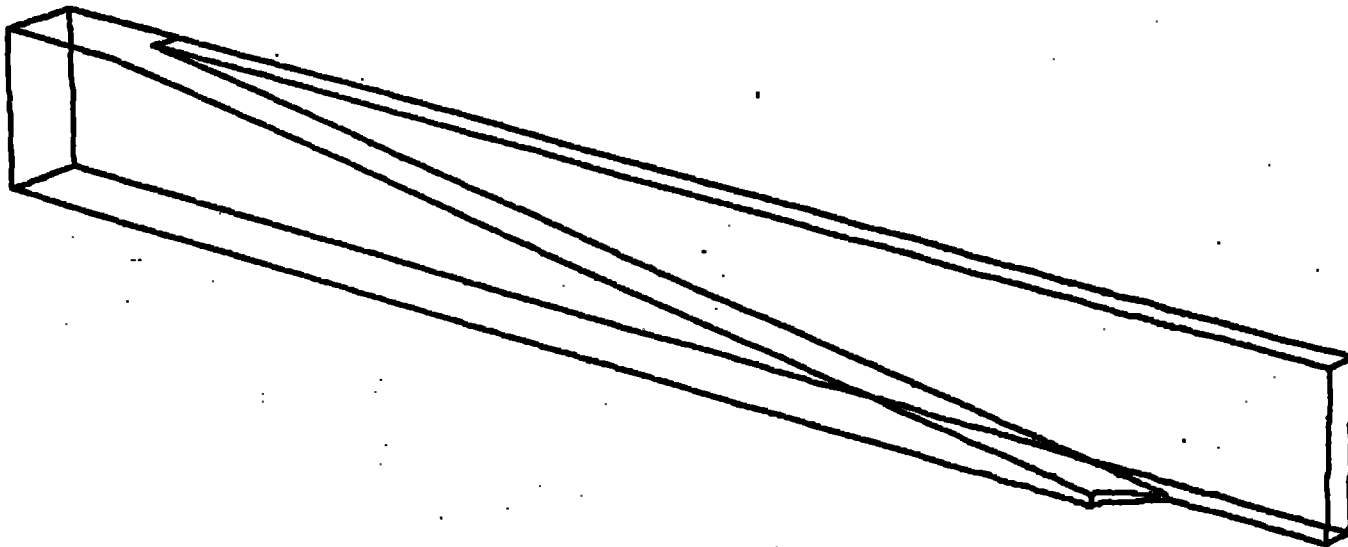$H = 1.9 \ W/CM^2$

MIN. NOSE HEIGHT = 11.71 MM
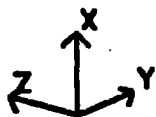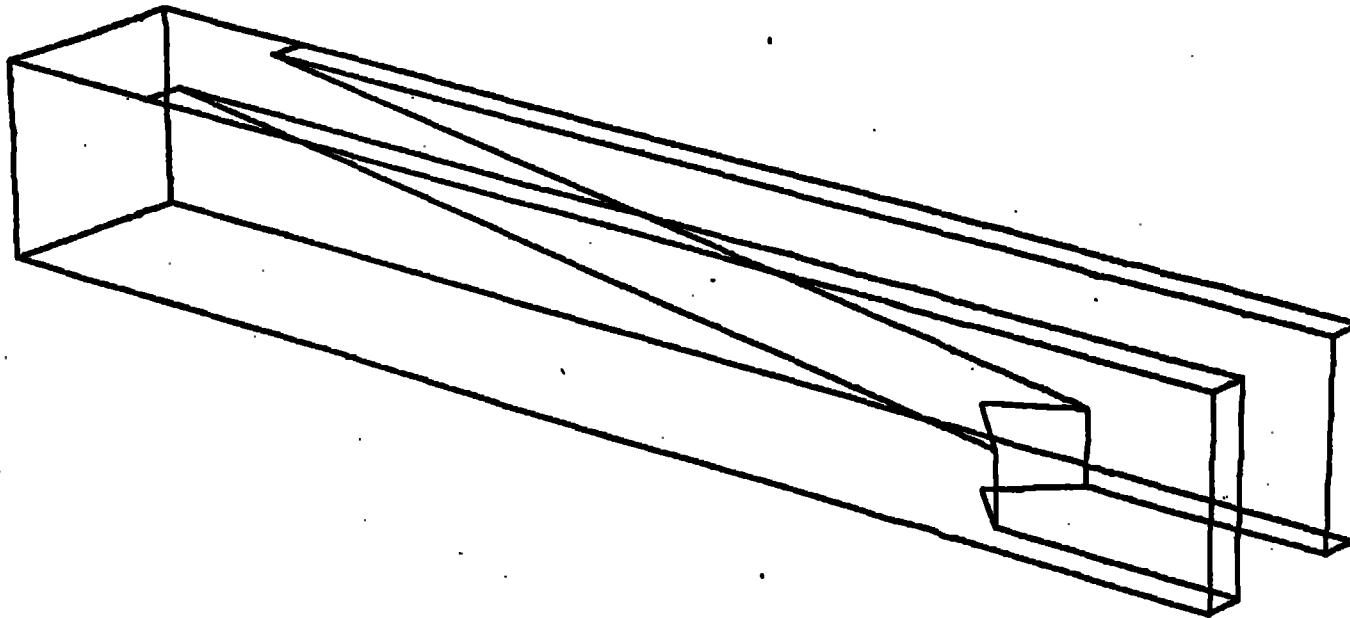
Figure 3. Schematic outline of the modeled part for the base geometry case (#2) studying the effect of asymmetric heating.

OUTLINE OF EDGES

CASE NO. 3 — UNDULATOR BEAM BASE CASE

$$H = 1.9 \ W/CM^2$$

MIN. NOSE HEIGHT = 11.71 MM

Figure 4. Schematic outline of the modeled part for the base geometry case (#3) studying the effect of undulator heating.

OUTLINE OF EDGES

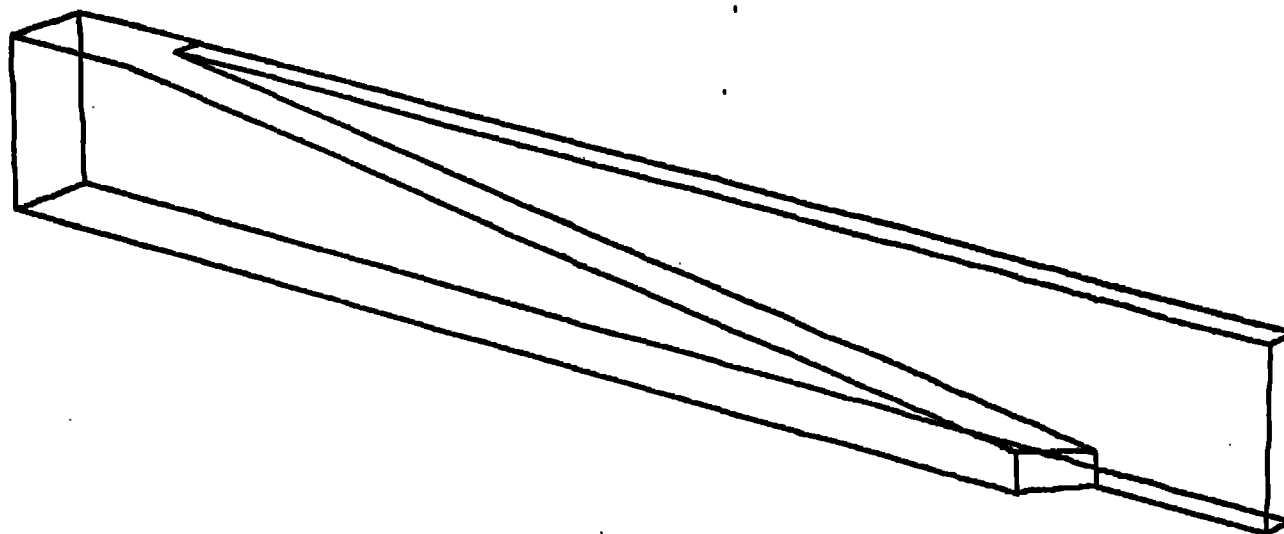CASE NO. 4 – LOW NOSE

$H = 1.9 \ W/CM^2$

MIN. NOSE HEIGHT. = 1.0 MM
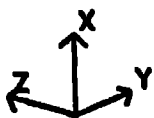
Figure 5. Schematic outline of the modeled part for the low-nose
geometry case (#4) studying the effect of nose height.

OUTLINE OF EDGES

CASE NO. 5 — MID NOSE

$$H = 1.9 \text{ W/CM}^2$$

MIN. NOSE HEIGHT. = 6.0 MM

Figure 6. Schematic outline of the modeled part for the mid-nose geometry (#5) case studying the effect of nose height.

THERMAL BOUNDARY CONDITIONS

CASE NO. 1 — BASE CASE WITH VARIABLE H

$H = 3.8, .38, 1.9$ W/CM^2

MIN. NOSE HEIGHT = 11.71 MM

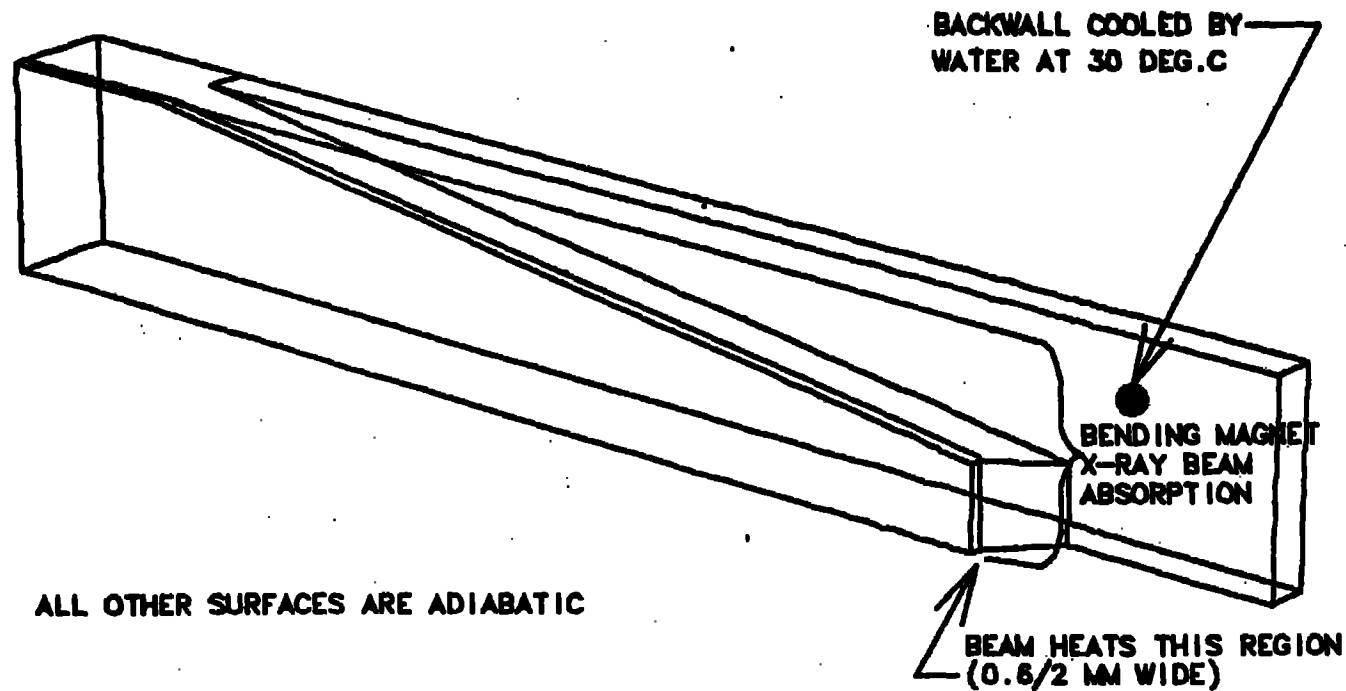BACKWALL COOLED BY
WATER AT 30 DEG.C

BENDING MAGNET
X-RAY BEAM
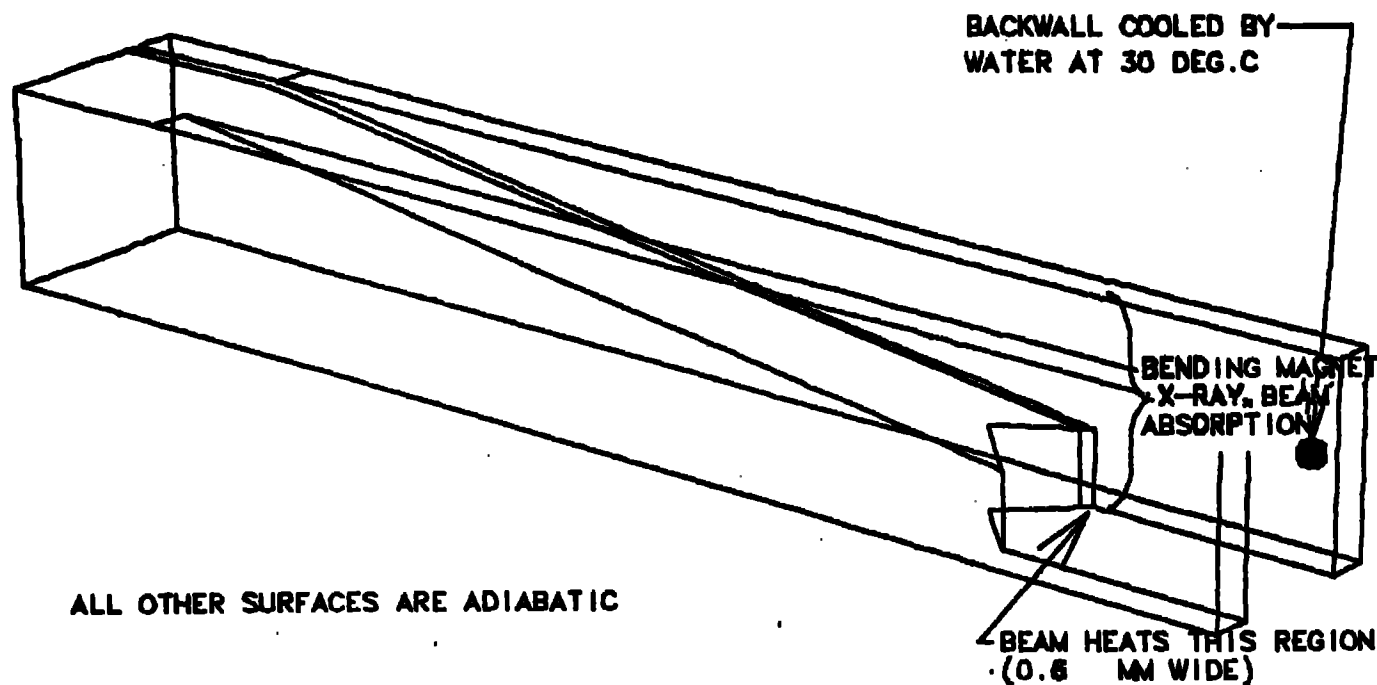ABSORPTION

ALL OTHER SURFACES ARE ADIABATIC

BEAM HEATS THIS REGION
(0.6/2 MM WIDE)

Figure 7. Thermal boundary conditions of the modeled part for the
base geometry case (#1) studying the effect of the heat
transfer coefficient.

THERMAL BOUNDARY CONDITIONS
CASE NO.2 — BENDING MAGNET BEAM OFFSTEER
$H = 1.9 \ W/CM^2$
MIN. NOSE HEIGHT = 11.71 MM

BACKWALL COOLED BY
WATER AT 30 DEG.C

BENDING MAGNET
X-RAY BEAM
ABSORPTION

ALL OTHER SURFACES ARE ADIABATIC
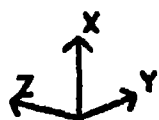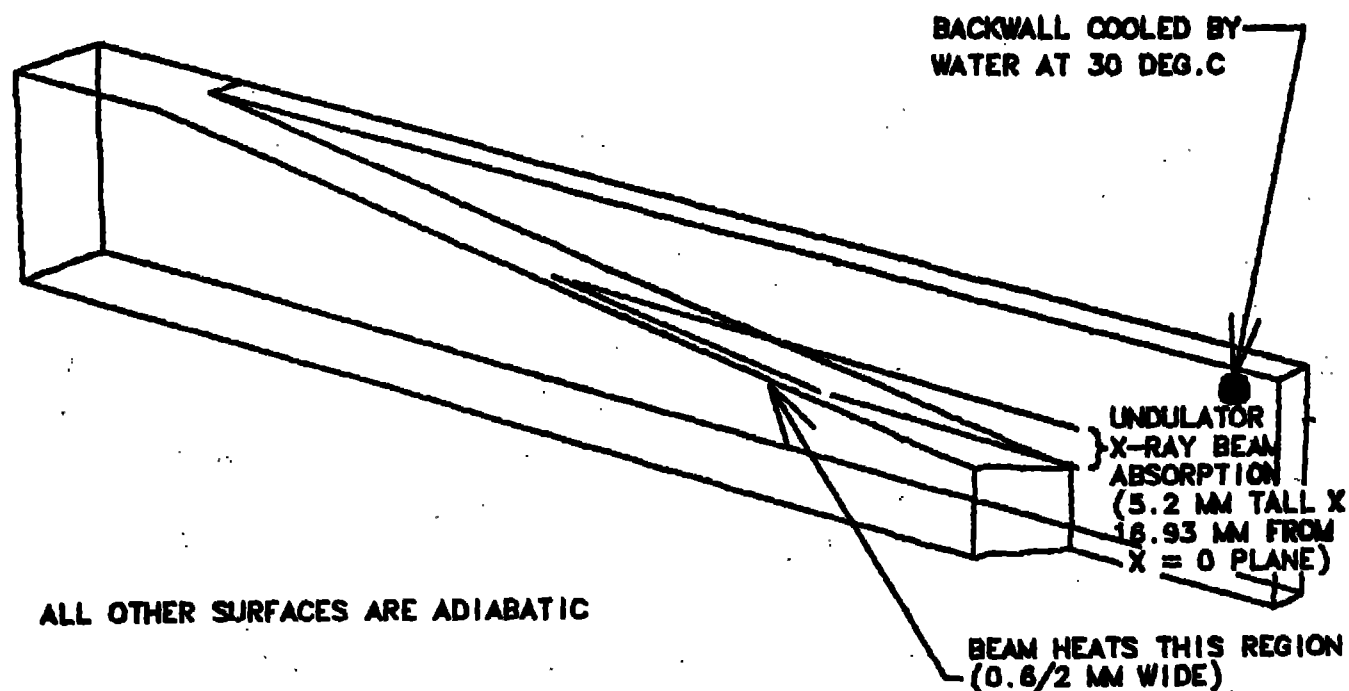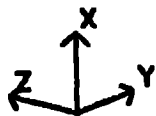
BEAM HEATS THIS REGION
(0.6 MM WIDE)

Figure 8. Thermal boundary conditions of the modeled part for the
base geometry case (#2) studying the effect of asymmetric
heating.

THERMAL BOUNDARY CONDITIONS
CASE NO. 3 — UNDULATOR BEAM BASE CASE
$$H = 1.9 \text{ W/CM}^2$$
$$\text{MIN. NOSE HEIGHT} = 11.71 \text{ MM}$$

BACKWALL COOLED BY
WATER AT 30 DEG.C

UNDULATOR
}X-RAY BEAM
ABSORPTION
(5.2 MM TALL X
16.93 MM FROM
X = 0 PLANE)

ALL OTHER SURFACES ARE ADIABATIC

BEAM HEATS THIS REGION
(0.6/2 MM WIDE)

Figure 9. Thermal boundary conditions of the modeled part for the
base geometry case (#3) studying the effect of undulator
heating.

THERMAL BOUNDARY CONDITIONS
CASE NO. 4 - LOW NOSE
$$H = 1.9 \ W/CM^2$$
$$MIN. \ NOSE \ HEIGHT. = 1.0 \ MM$$

BACKWALL COOLED BY
WATER AT 30 DEG.C

BEND.MAGNET
X-RAY BEAM
ABSORPTION

ALL OTHER SURFACES ARE ADIABATIC
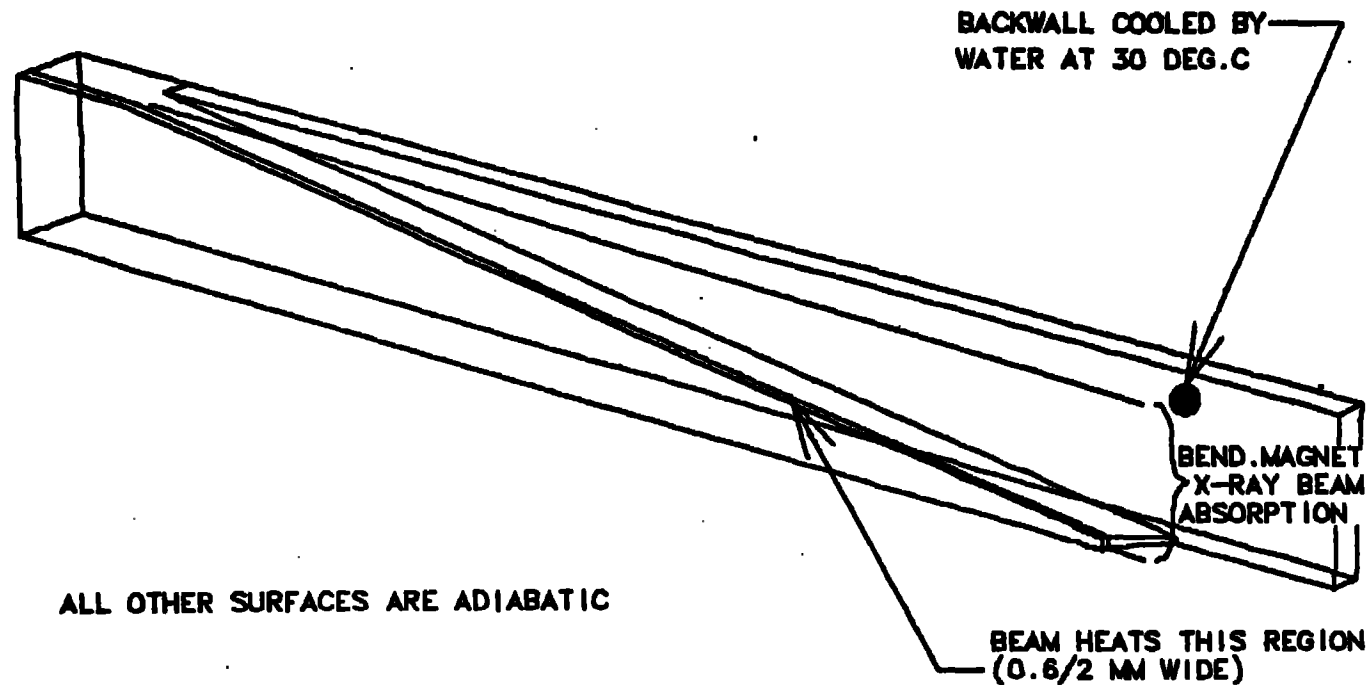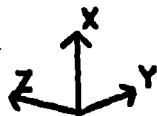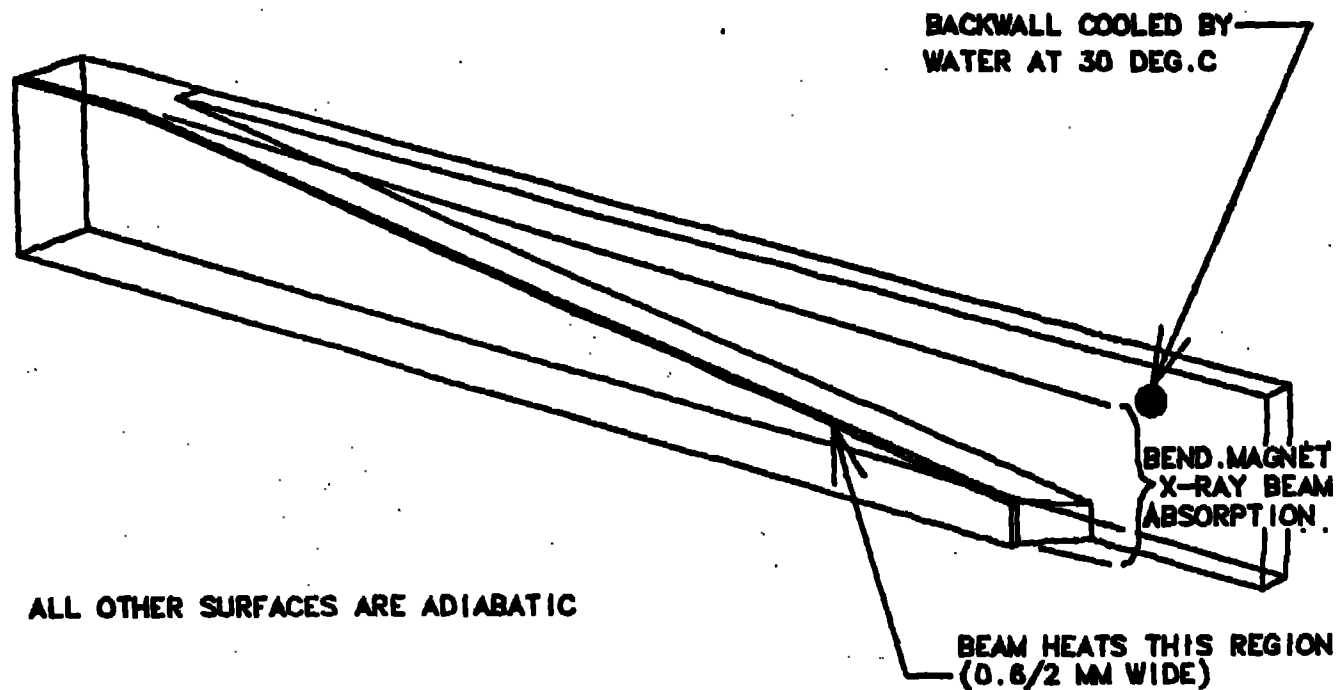
BEAM HEATS THIS REGION
(0.6/2 MM WIDE)

Figure 10. Thermal boundary conditions of the modeled part for the
low-nose geometry case (#4) studying the effect of nose
height.

THERMAL BOUNDARY CONDITIONS
CASE NO. 5 – MID NOSE

$$H = 1.9 \text{ W/CM}^2$$

$$\text{MIN. NOSE HEIGHT.} = 6.0 \text{ MM}$$

BACKWALL COOLED BY WATER AT 30 DEG.C

BEND.MAGNET X-RAY BEAM ABSORPTION.

ALL OTHER SURFACES ARE ADIABATIC

BEAM HEATS THIS REGION (0.6/2 MM WIDE)

Figure 11. Thermal boundary conditions of the modeled part for the mid-nose geometry (#5) case studying the effect of nose height.

STRUCTURAL BOUNDARY CONDITIONS
CASE NO. 1 — BASE CASE WITH VARIABLE H
$H = 3.8, .38, 1.9 \ W/CM^2$
MIN. NOSE HEIGHT = 11.71 MM

REAR PLANE
NO Z
DISPLACEMENT

CENTERPLANE
NO Y DISPLACEMENT

CORNER
NO X DISPLACEMENT

ALL OTHER SURFACES ARE UNRESTRAINED
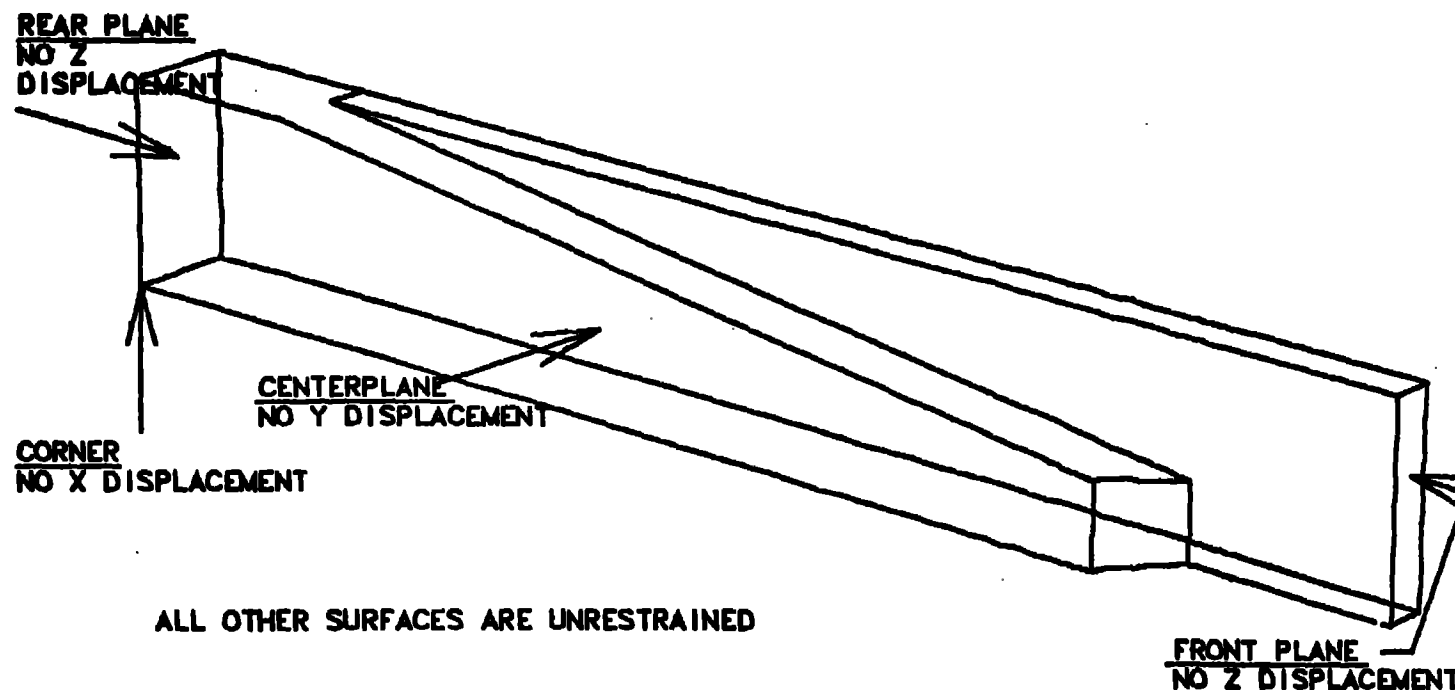
FRONT PLANE
NO Z DISPLACEMENT

X

Z Y
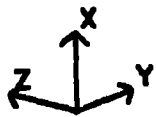
Figure 12. Displacement structural boundary conditions of the modeled
part for the base geometry case (#1) studying the effect
of the heat transfer coefficient.

STRUCTURAL BOUNDARY CONDITIONS
CASE NO.2 — BENDING MAGNET BEAM OFFSTEER
$H = 1.9 \ W/CM^2$
MIN. NOSE HEIGHT = 11.71 MM

REAR PLANE
NO Z
DISPLACEMENT

SIDE PLANE
OPPOSITE THE OFF-
STEERED BEAM STRIKE
NO Y DISPLACEMENT

CORNER
NO X DISPLACEMENT

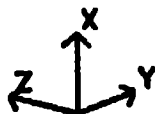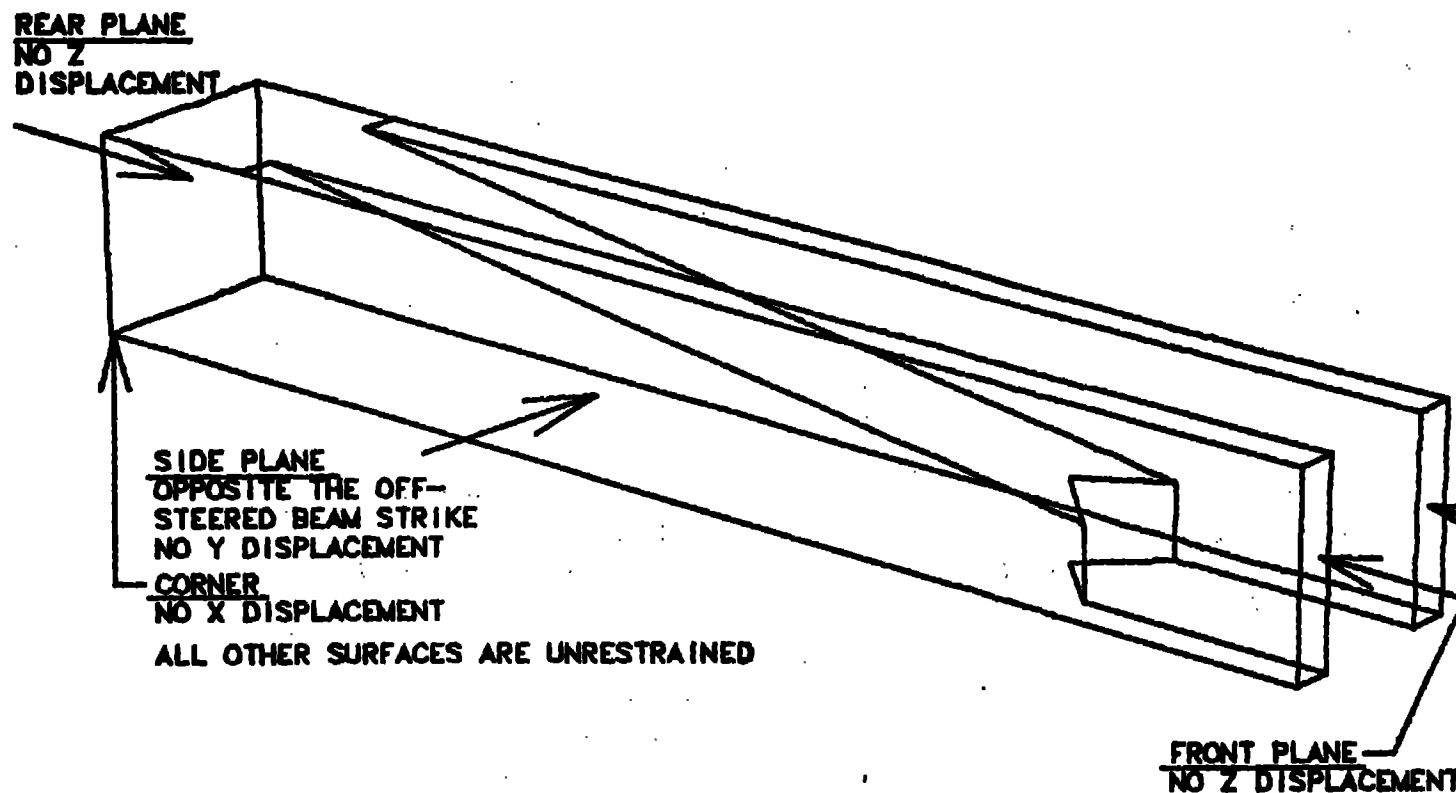ALL OTHER SURFACES ARE UNRESTRAINED

FRONT PLANE
NO Z DISPLACEMENT

Figure 13. Displacement structural boundary conditions of the modeled
part for the base geometry case (#2) studying the effect
of asymmetric heating.

STRUCTURAL BOUNDARY CONDITIONS
CASE NO. 3 – UNDULATOR BEAM BASE CASE
$$H = 1.9 \ W/CM^2$$
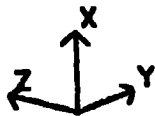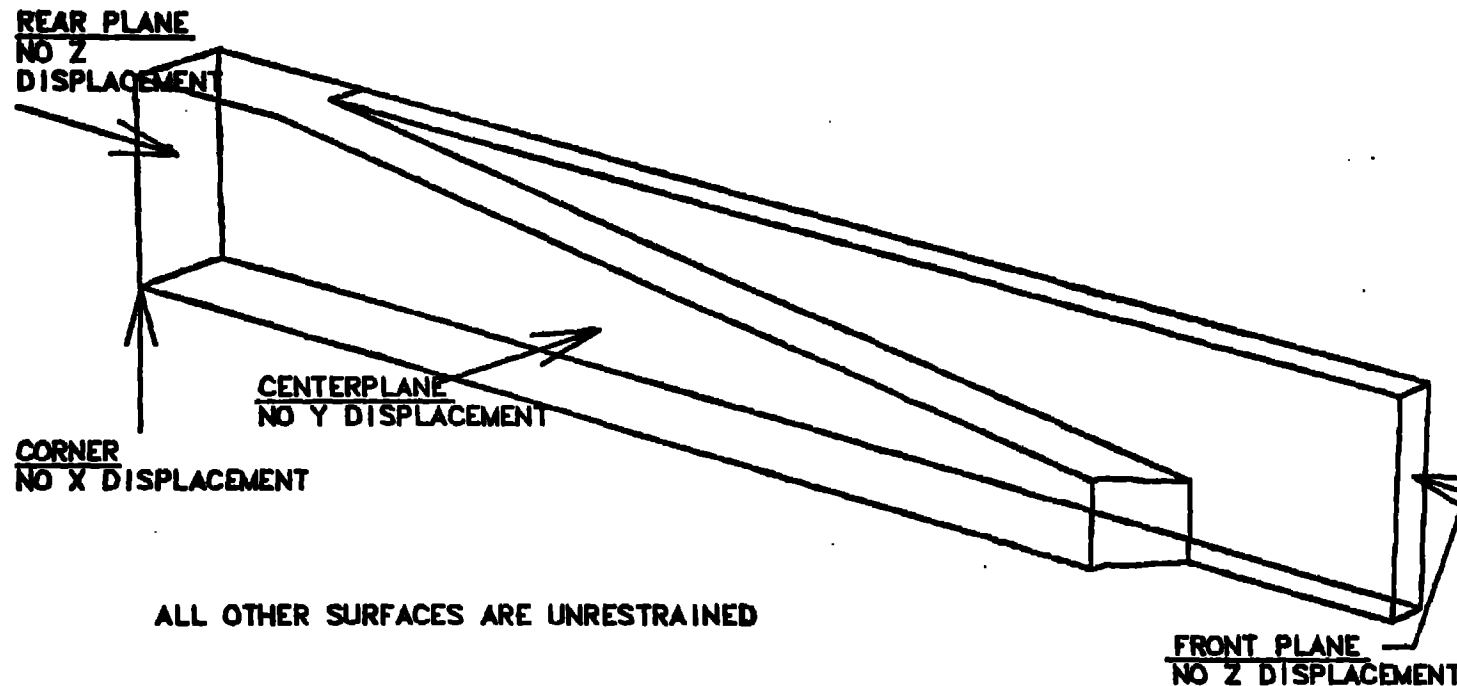$$MIN. \ NOSE \ HEIGHT = 11.71 \ MM$$

Figure 14. Displacement structural boundary conditions of the modeled
part for the base geometry case (#3) studying the effect
of undulator heating.

STRUCTURAL BOUNDARY CONDITIONS
CASE NO. 4 — LOW NOSE

$$H = 1.9 \ W/CM^2$$

$$MIN. \ NOSE \ HEIGHT. = 1.0 \ MM$$

REAR PLANE
NO Z
DISPLACEMENT

CENTERPLANE
NO Y DISPLACEMENT

CORNER
NO X DISPLACEMENT

ALL OTHER SURFACES ARE UNRESTRAINED

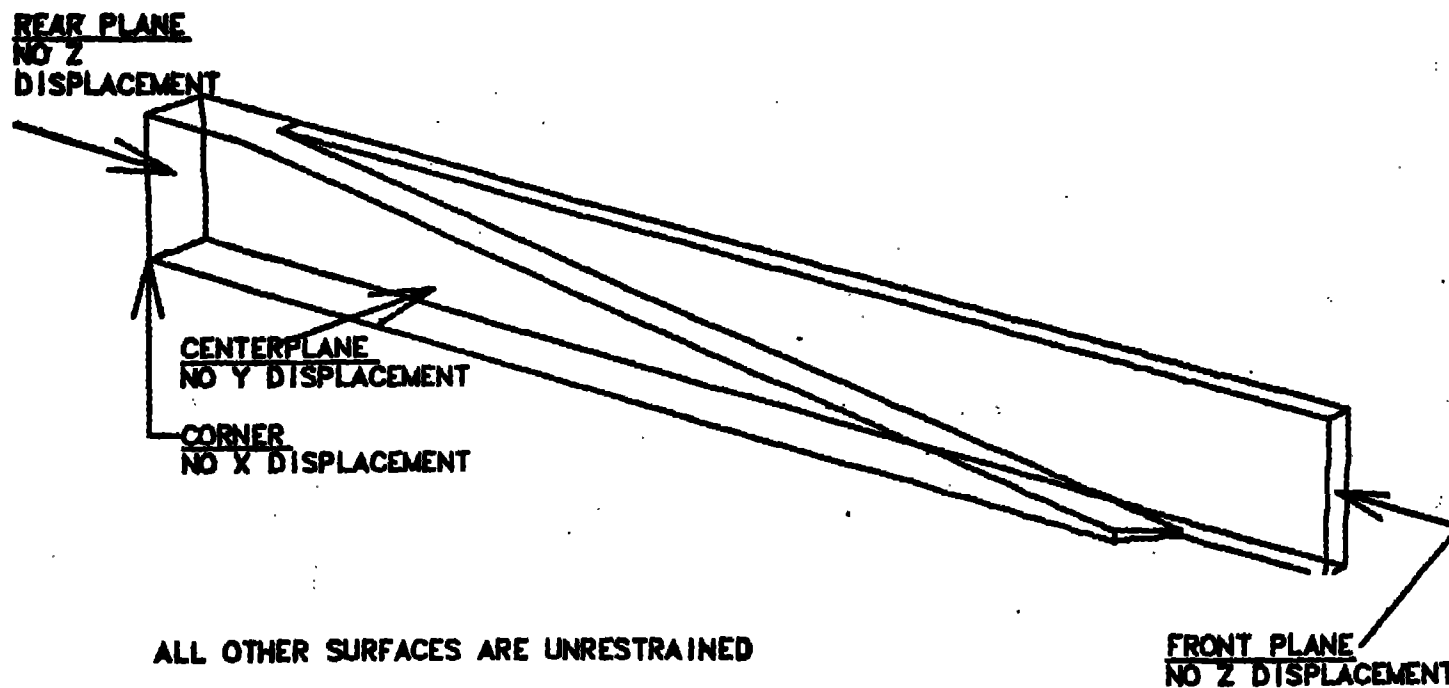FRONT PLANE
NO Z DISPLACEMENT

X
Z Y

Figure 15. Displacement structural boundary conditions of the modeled
part for the low-nose geometry case (#4) studying the
effect of nose height.

STRUCTURAL BOUNDARY CONDITIONS
CASE NO. 5 — MID NOSE

$$H = 1.9 \ W/CM^2$$

MIN. NOSE HEIGHT. = 6.0 MM

REAR PLANE
NO Z
DISPLACEMENT

CENTER PLANE
NO Y DISPLACEMENT

CORNER
NO X DISPLACEMENT

ALL OTHER SURFACES ARE UNRESTRAINED
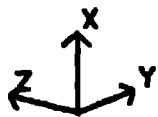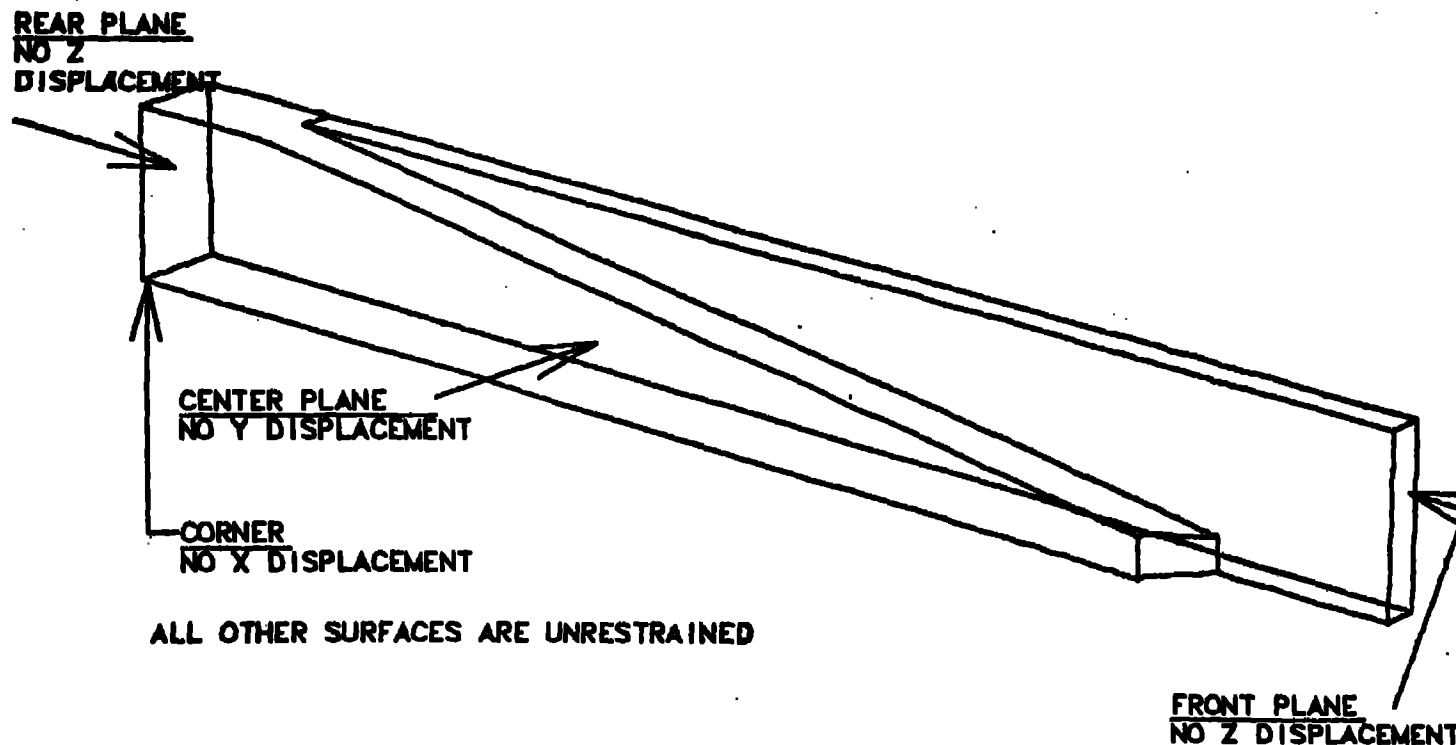
FRONT PLANE
NO Z DISPLACEMENT

X

Z   Y

Figure 16. Displacement structural boundary conditions of the modeled
part for the mid-nose geometry (#5) case studying the
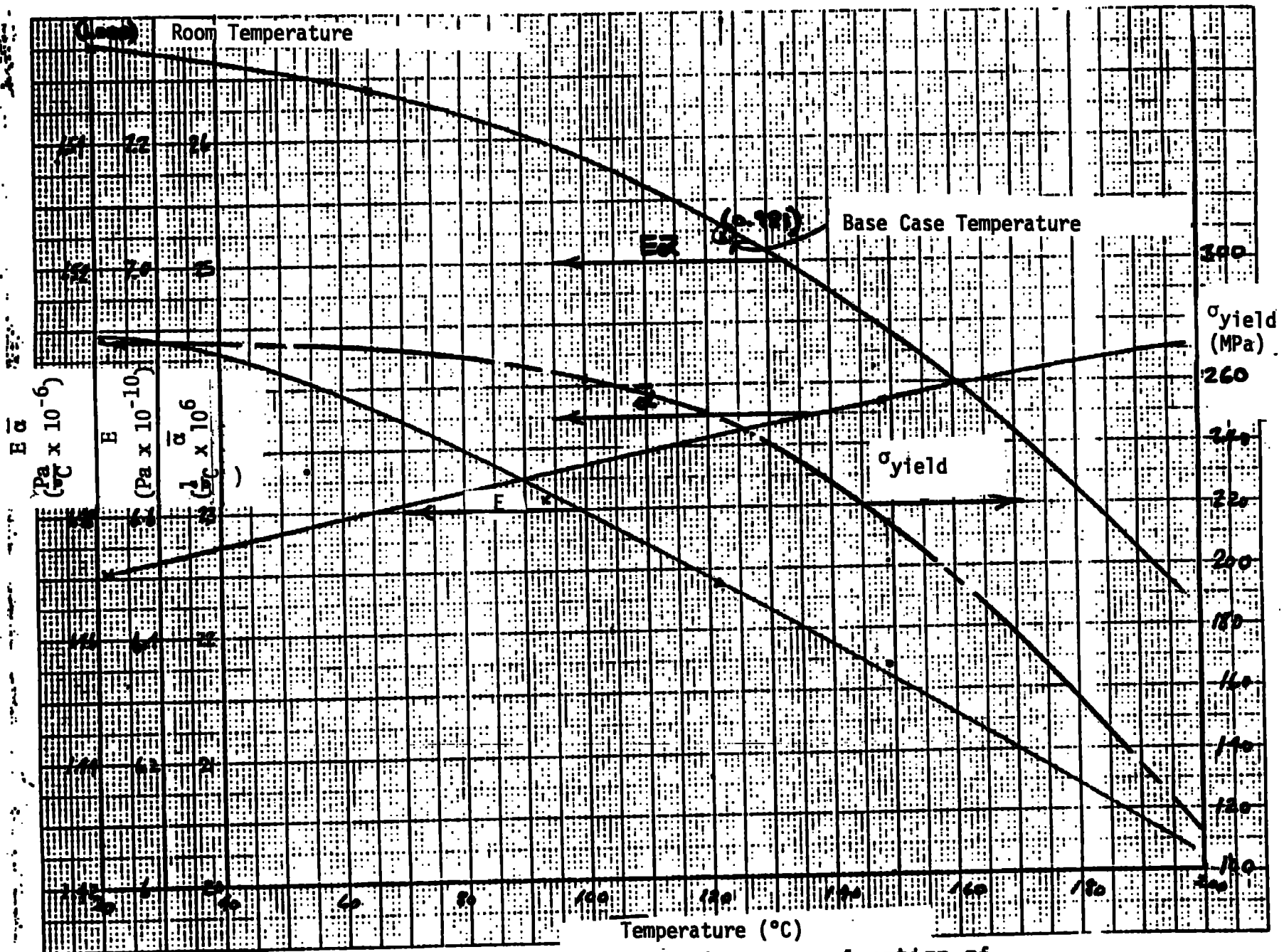effect of nose height.

Figure 17. Structural properties of 6061-T6 aluminum as a function of temperature.

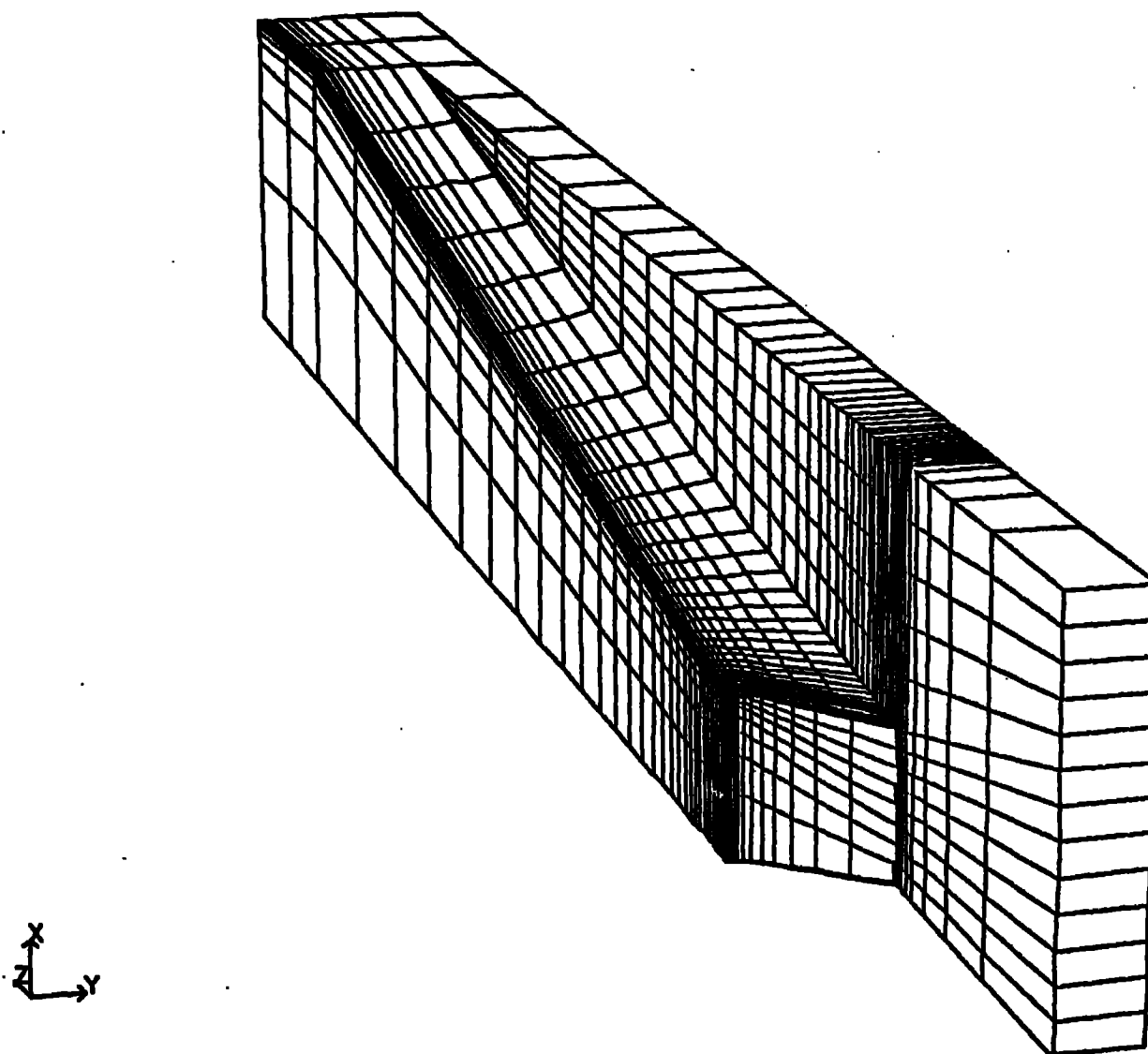SLAC DIVERTOR CROTCH/CASE 1D/BASEBM + 1.9 W/CM2/
TIME WORD = 1.00000E+20

Figure 18. Schematic of the zoning for the finite element analyses of
the base geometry case (#1) studying the effect of the
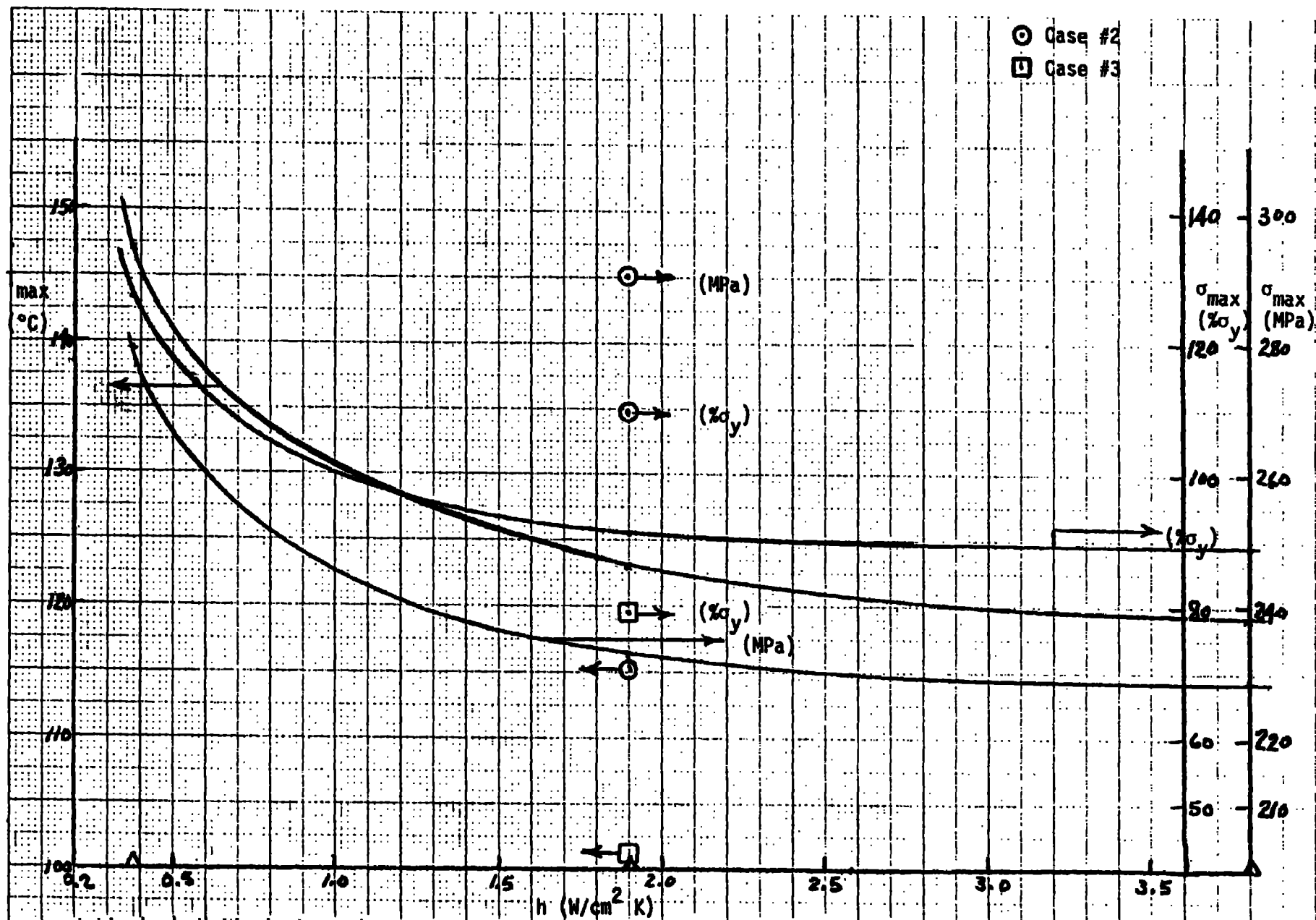heat transfer coefficient.

Figure 19. Maximum temperature and maximum stress vs heat transfer coefficient for base geometry case (#1) with a min. nose height of 11.71 mm.
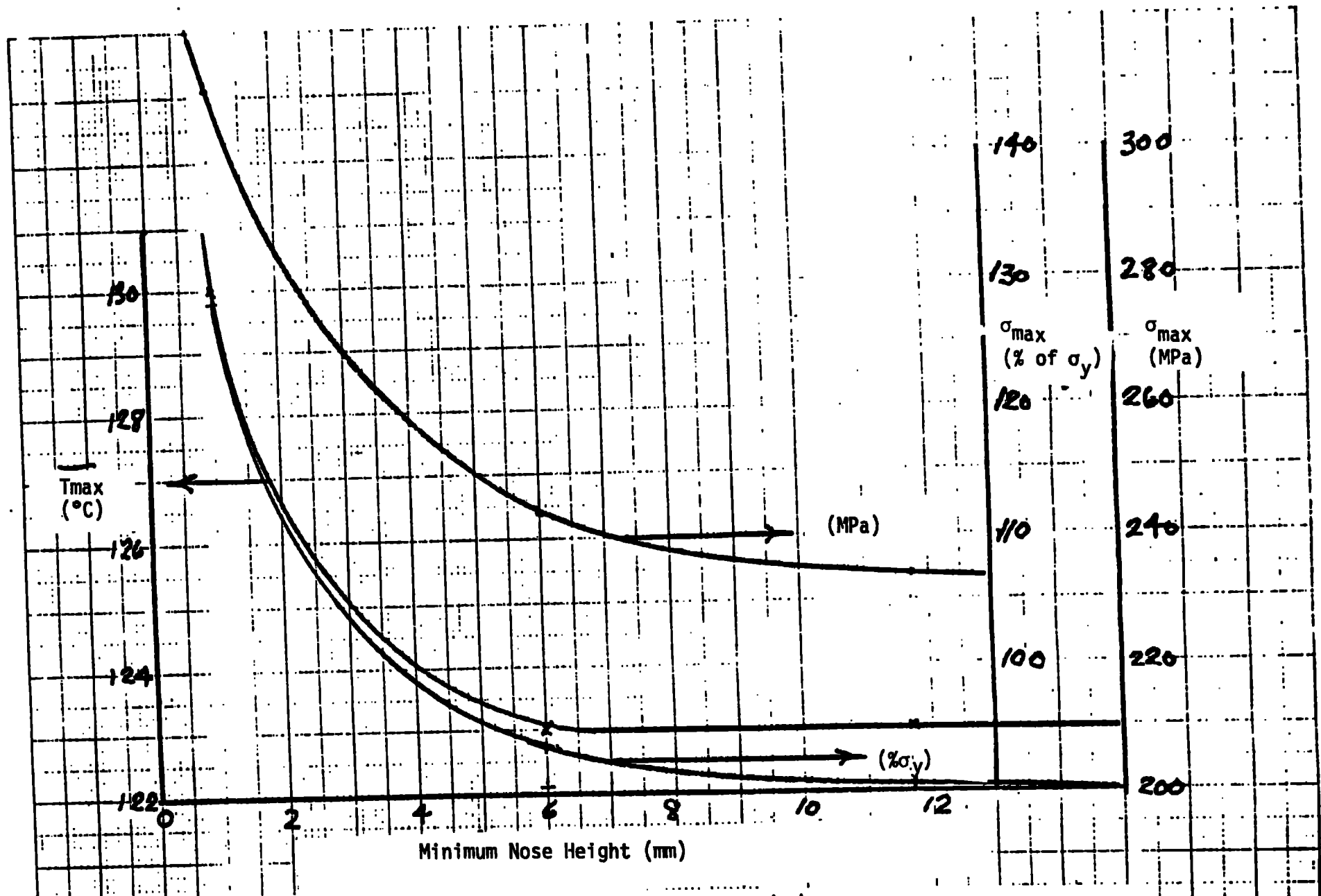
Figure 20. Maximum temperature and maximum stress vs minimum nose height for the most probable heat transfer coefficient (i.e. h=1.9 W/cm^2).

SLAC DIVERTOR CROTCH/CASE 1A/BASEBM + 3.8 W/CM2/

TIME WORD = 1.00000E+20

CONTOURS OF TEMPERATURE

MIN= .300E+02 AT NODE 4864
MAX= .119E+03 AT NODE   6

CONTOUR VALUES(°C)
A= 3.00E+01
B= 3.50E+01
C= 4.00E+01
D= 4.50E+01
E= 5.00E+01
F= 5.50E+01
G= 6.00E+01
H= 6.50E+01
I= 7.00E+01
J= 7.50E+01
K= 8.00E+01
L= 8.50E+01
M= 9.00E+01
N= 9.50E+01
O= 1.00E+02
P= 1.05E+02
Q= 1.10E+02
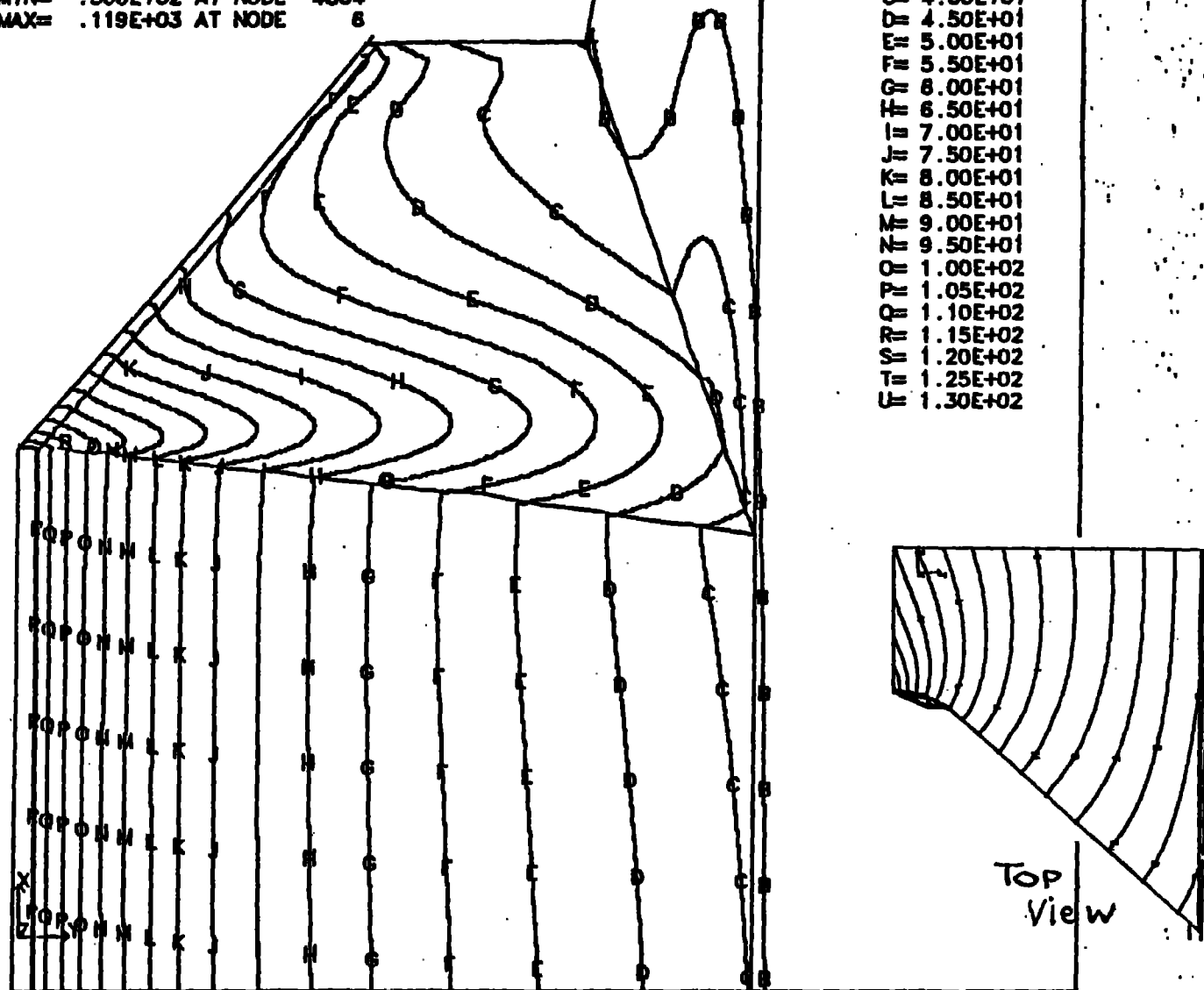R= 1.15E+02
S= 1.20E+02
T= 1.25E+02
U= 1.30E+02

Top
View

Figure 21. Isotherm plot (front view) of the modeled part for the
base geometry case (#1A) studying the effect of the heat
transfer coefficient, h=3.8 W/cm^2.

SLAC DIVERTOR CROTCH/CASE 1B/BASEBM + .38 W/CM2/

TIME WORD = 1.00000E+20

CONTOURS OF TEMPERATURE

MIN= .357E+02 AT NODE 4869
MAX= .147E+03 AT NODE 1

CONTOUR VALUES(°C)
A= 3.00E+01
B= 3.50E+01
C= 4.00E+01
D= 4.50E+01
E= 5.00E+01
F= 5.50E+01
G= 6.00E+01
H= 6.50E+01
I= 7.00E+01
J= 7.50E+01
K= 8.00E+01
L= 8.50E+01
M= 9.00E+01
N= 9.50E+01
O= 1.00E+02
P= 1.05E+02
Q= 1.10E+02
R= 1.15E+02
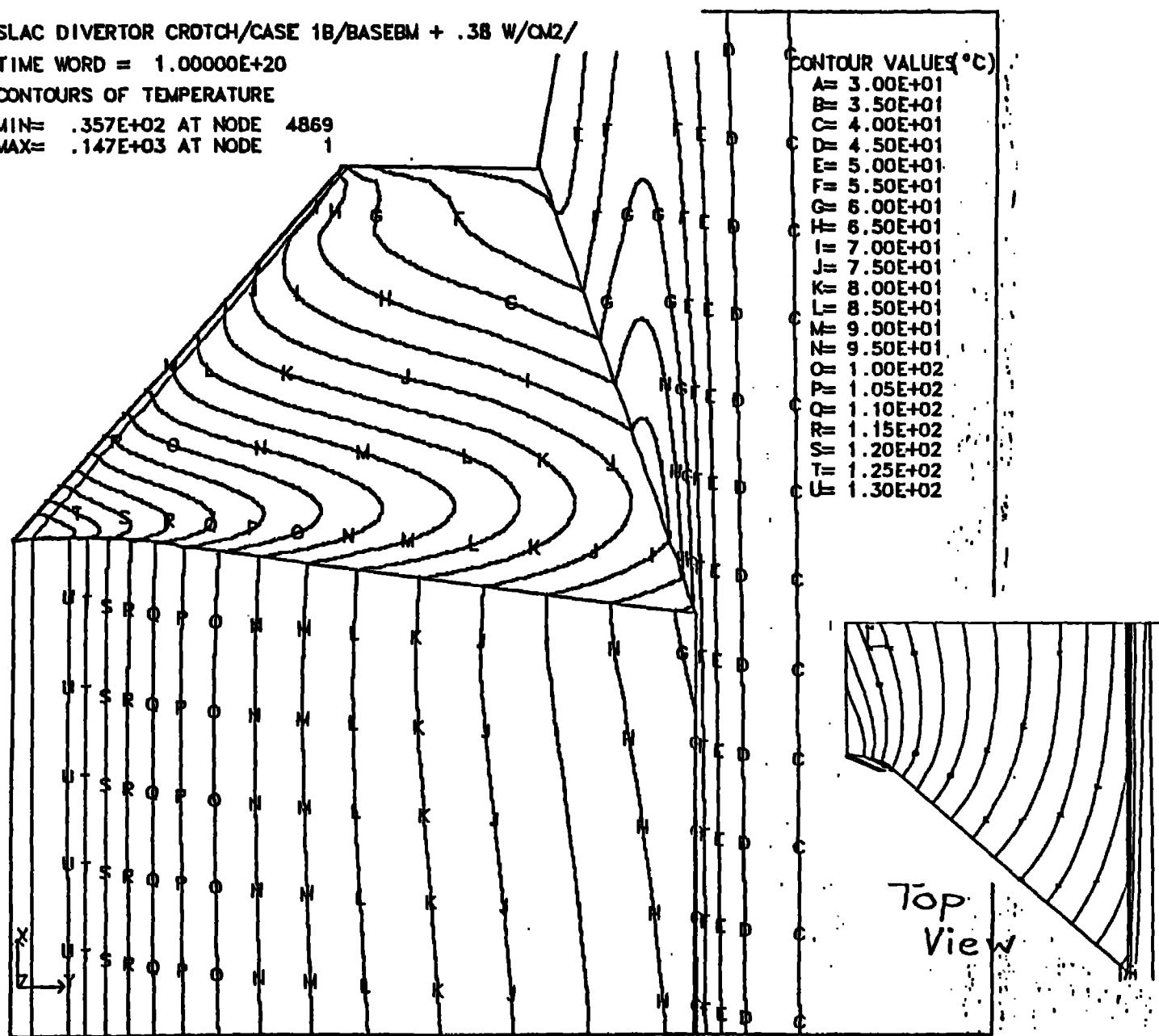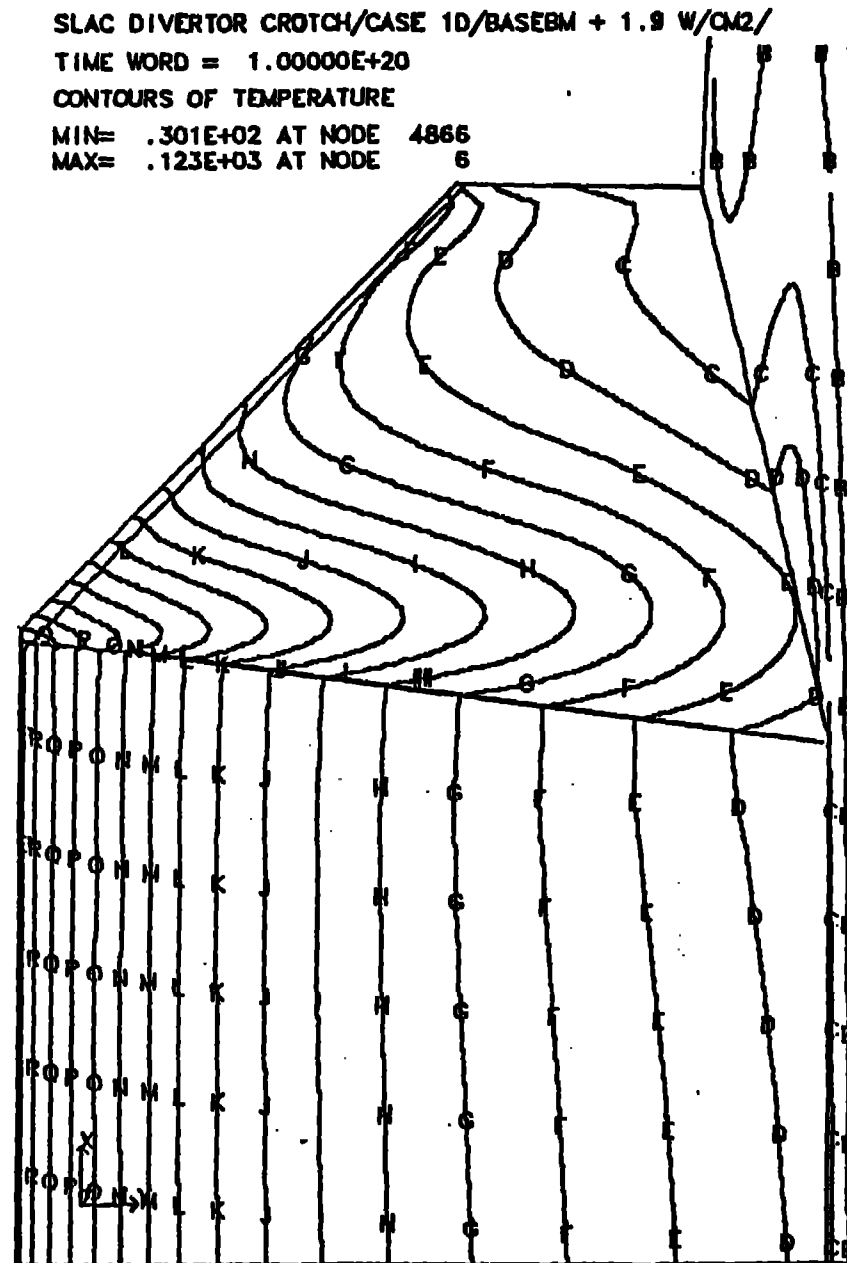S= 1.20E+02
T= 1.25E+02
U= 1.30E+02

Top
View

Figure 22. Isotherm plot (front view) of the modeled part for the
base geometry case (#1B) studying the effect of the heat
transfer coefficient, h=0.38 W/cm^2.

SLAC DIVERTOR CROTCH/CASE 1D/BASEBM + 1.9 W/CM2/

TIME WORD = 1.00000E+20

CONTOURS OF TEMPERATURE

MIN= .301E+02 AT NODE 4866
MAX= .123E+03 AT NODE   6

CONTOUR VALUES
A= 3.00E+01(°C)
B= 3.50E+01
C= 4.00E+01
D= 4.50E+01
E= 5.00E+01
F= 5.50E+01
G= 6.00E+01
H= 6.50E+01
I= 7.00E+01
J= 7.50E+01
K= 8.00E+01
L= 8.50E+01
M= 9.00E+01
N= 9.50E+01
O= 1.00E+02
P= 1.05E+02
Q= 1.10E+02
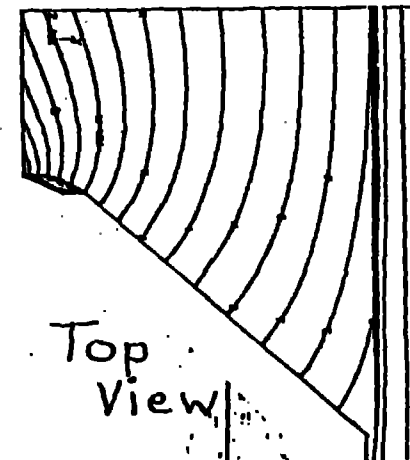R= 1.15E+02
S= 1.20E+02
T= 1.25E+02
U= 1.30E+02

Top View

Figure 23. Isotherm plot (front view) of the modeled part for the
base geometry case (#1D) studying the effect of the heat
transfer coefficient, h=1.9 W/cm^2.

SLAC DIVERTOR CROTCH/CASE 2/FULL SIDE STRIKE /T

TIME WORD = 1.00000E+20

CONTOURS OF TEMPERATURE

MIN= .294E+02 AT NODE 188
MAX= .116E+03 AT NODE 1287

CONTOUR VALUES
A= 3.00E+01 (°C)
B= 3.50E+01
C= 4.00E+01
D= 4.50E+01
E= 5.00E+01
F= 5.50E+01
G= 6.00E+01
H= 6.50E+01
I= 7.00E+01
J= 7.50E+01
K= 8.00E+01
L= 8.50E+01
M= 9.00E+01
N= 9.50E+01
O= 1.00E+02
P= 1.05E+02
Q= 1.10E+02
R= 1.15E+02
S= 1.20E+02
T= 1.25E+02
U= 1.30E+02

Top
View
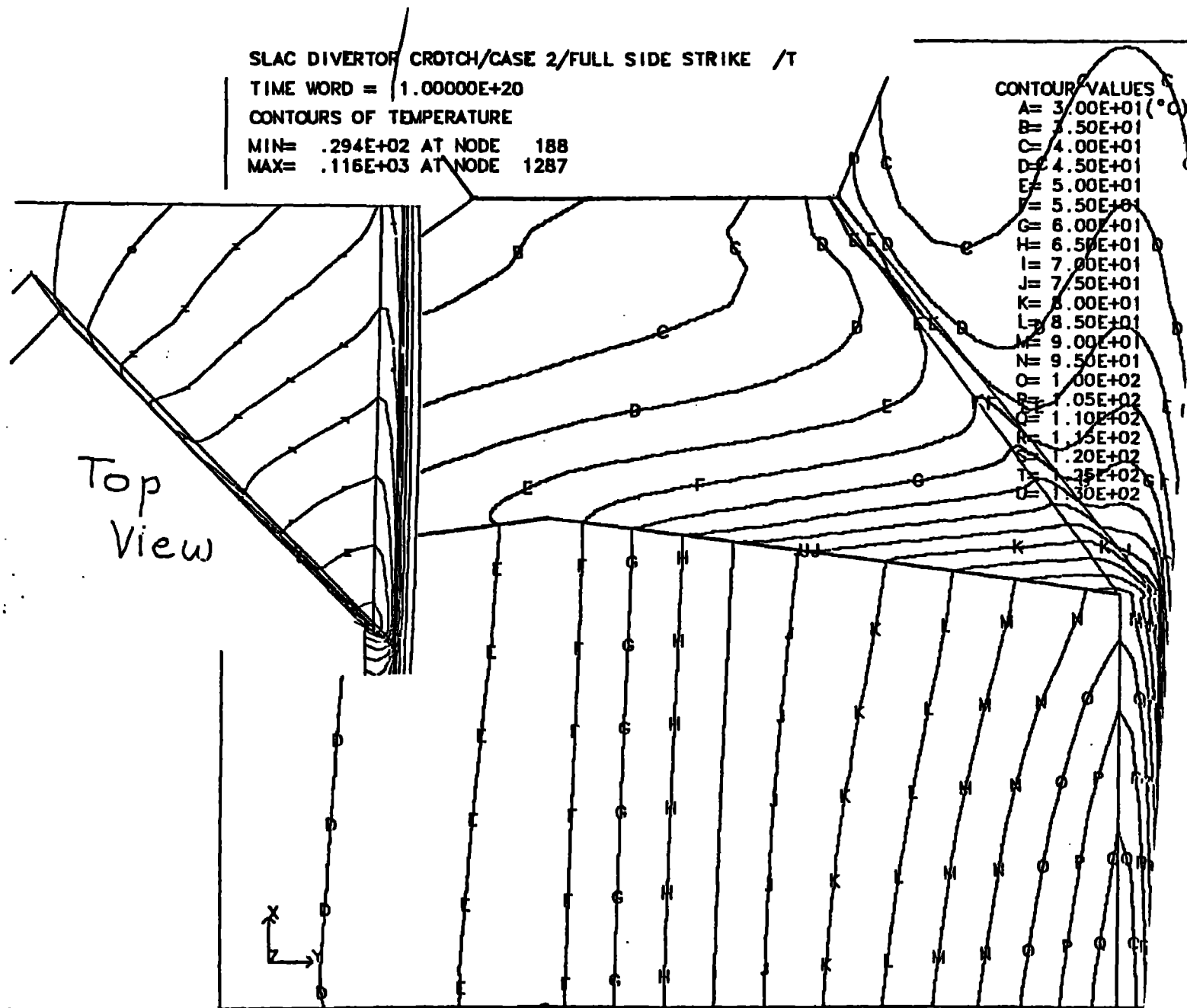
Figure 24. Isotherm plot (front view) of the modeled part for the
base geometry case (#2) studying the effect of asymmetric
heating.

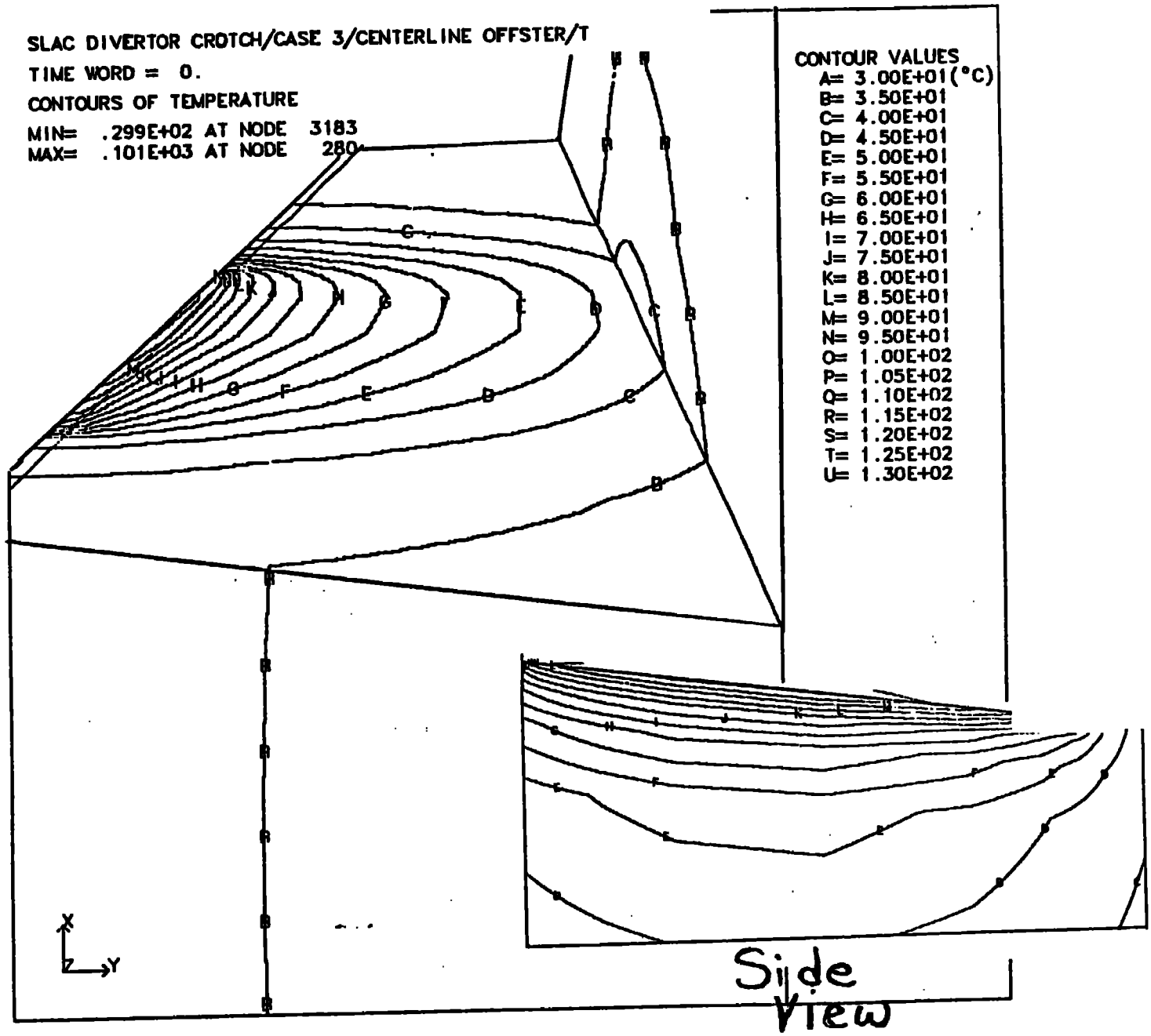SLAC DIVERTOR CROTCH/CASE 3/CENTERLINE OFFSTER/T

TIME WORD = 0.

CONTOURS OF TEMPERATURE

MIN= .299E+02 AT NODE 3183
MAX= .101E+03 AT NODE   280

CONTOUR VALUES
A= 3.00E+01(°C)
B= 3.50E+01
C= 4.00E+01
D= 4.50E+01
E= 5.00E+01
F= 5.50E+01
G= 6.00E+01
H= 6.50E+01
I= 7.00E+01
J= 7.50E+01
K= 8.00E+01
L= 8.50E+01
M= 9.00E+01
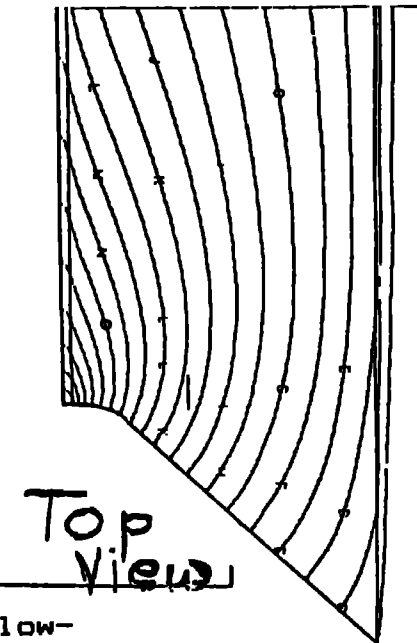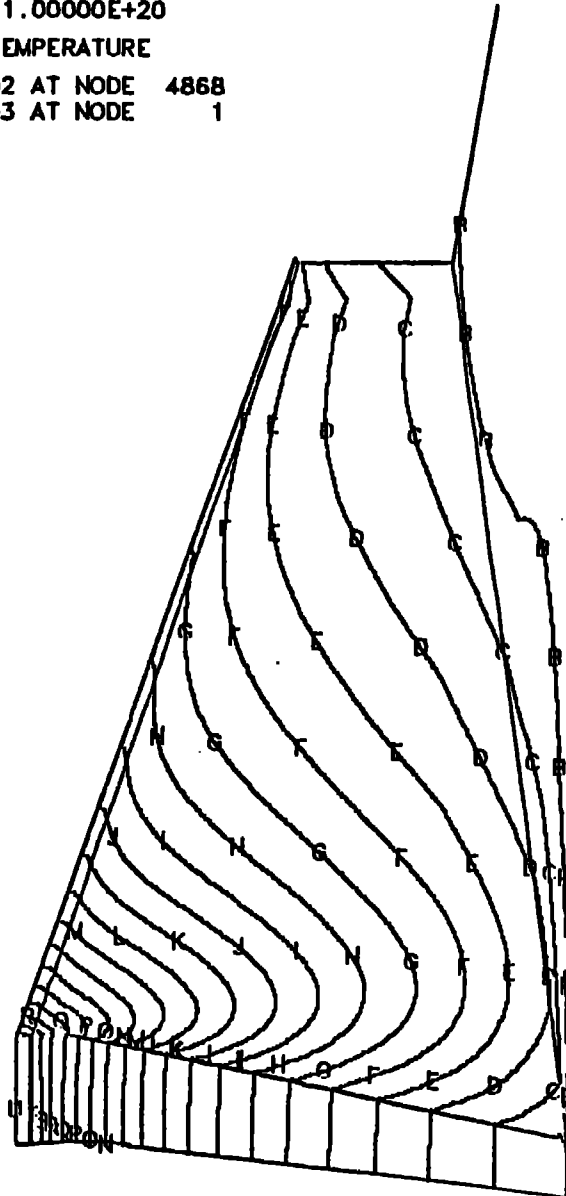N= 9.50E+01
O= 1.00E+02
P= 1.05E+02
Q= 1.10E+02
R= 1.15E+02
S= 1.20E+02
T= 1.25E+02
U= 1.30E+02

Side
View

Figure 25. Isotherm plot (front view) of the modeled part for the
base geometry case (#3) studying the effect of undulator
heating.

SLAC DIVERTOR CROTCH/CASE 4/LOWNOSE + 1.9 W/CM2/
TIME WORD = 1.00000E+20
CONTOURS OF TEMPERATURE

MIN= .300E+02 AT NODE 4868
MAX= .130E+03 AT NODE 1

CONTOUR VALUES
A= 3.00E+01(°C)
B= 3.50E+01
C= 4.00E+01
D= 4.50E+01
E= 5.00E+01
F= 5.50E+01
G= 6.00E+01
H= 6.50E+01
I= 7.00E+01
J= 7.50E+01
K= 8.00E+01
L= 8.50E+01
M= 9.00E+01
N= 9.50E+01
O= 1.00E+02
P= 1.05E+02
Q= 1.10E+02
R= 1.15E+02
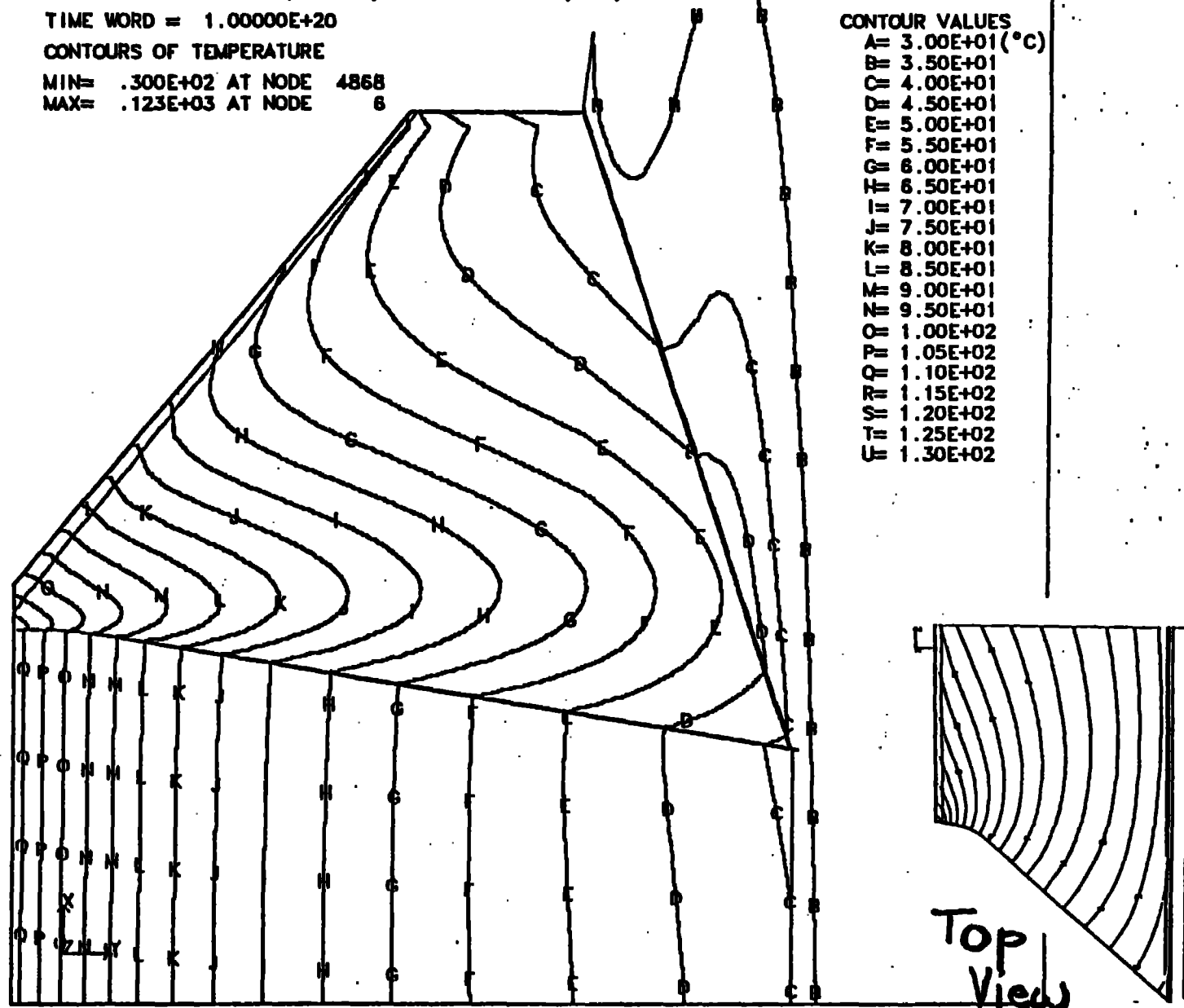S= 1.20E+02
T= 1.25E+02
U= 1.30E+02

Top View

Figure 26. Isotherm plot (front view) of the modeled part for the low-
nose geometry case (#4) studying the effect of nose
height, (minimum nose height=1 mm).

SLAC DIVERTOR CROTCH/CASE 5/MIDNOSE + 1.9 W/CM2/

TIME WORD = 1.00000E+20

CONTOURS OF TEMPERATURE

MIN= .300E+02 AT NODE 4868
MAX= .123E+03 AT NODE 6

CONTOUR VALUES
A= 3.00E+01(°C)
B= 3.50E+01
C= 4.00E+01
D= 4.50E+01
E= 5.00E+01
F= 5.50E+01
G= 6.00E+01
H= 6.50E+01
I= 7.00E+01
J= 7.50E+01
K= 8.00E+01
L= 8.50E+01
M= 9.00E+01
N= 9.50E+01
O= 1.00E+02
P= 1.05E+02
Q= 1.10E+02
R= 1.15E+02
S= 1.20E+02
T= 1.25E+02
U= 1.30E+02

Top View

Figure 27. Isotherm plot (front view) of the modeled part for the mid-nose geometry (#5) case studying the effect of nose height, (minimum nose height=6 mm).

SLAC DIVERTOR CROTCH/CASE 1A/BASEBM + 3.8 W/CM2/TACO3D&GEMIN

TIME WORD = 1.00000E+00

CONTOURS OF EFF. STRESS (V-M)

MIN= .715E+07 IN ELEMENT 759
MAX= .228E+09 IN ELEMENT 312

CONTOUR VALUES
A= 0.   (PA)
B= 2.00E+07
C= 4.00E+07
D= 6.00E+07
E= 8.00E+07
F= 1.00E+08
G= 1.20E+08
H= 1.40E+08
I= 1.60E+08
J= 1.80E+08
K= 2.00E+08
L= 2.20E+08
M= 2.40E+08
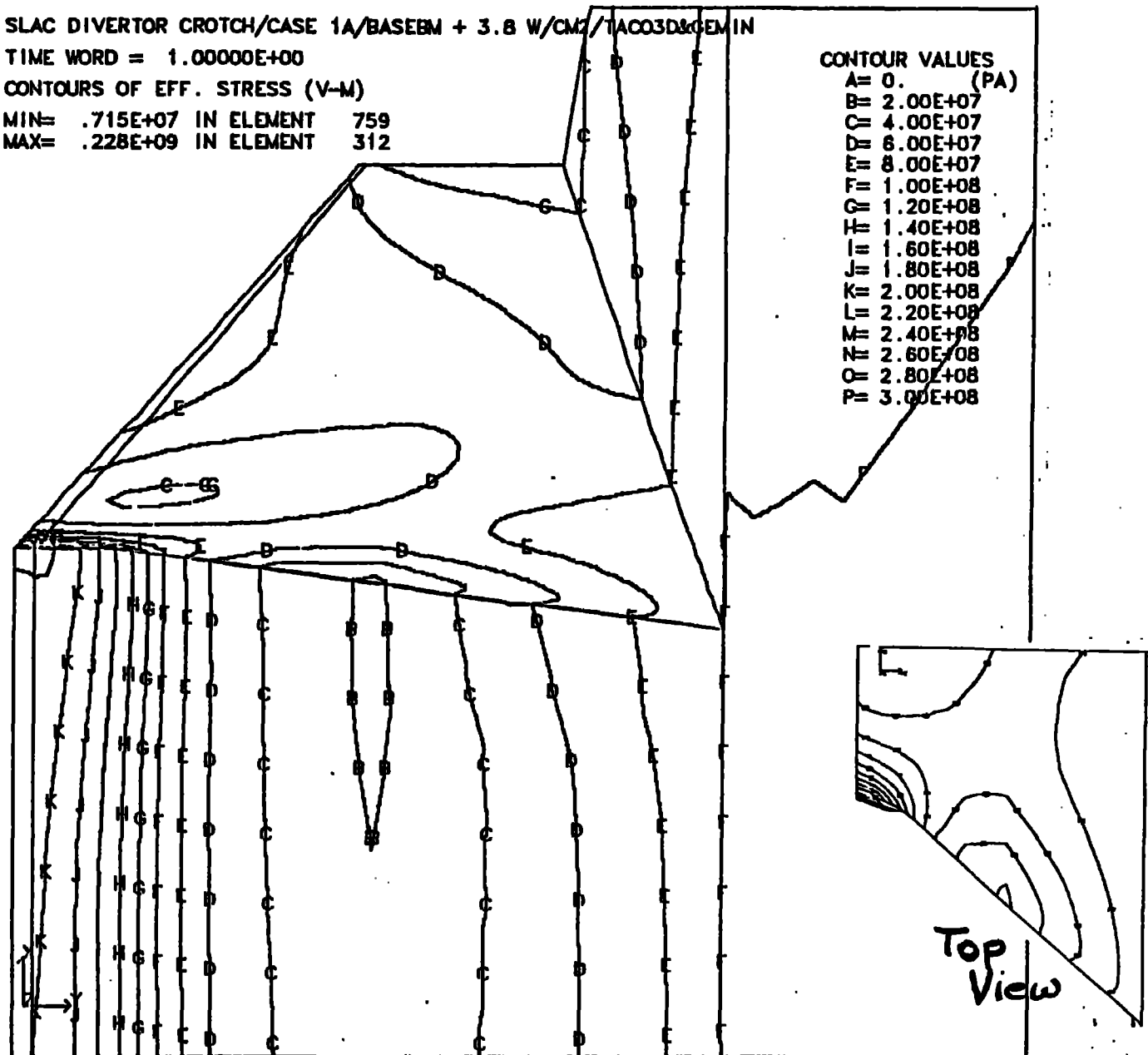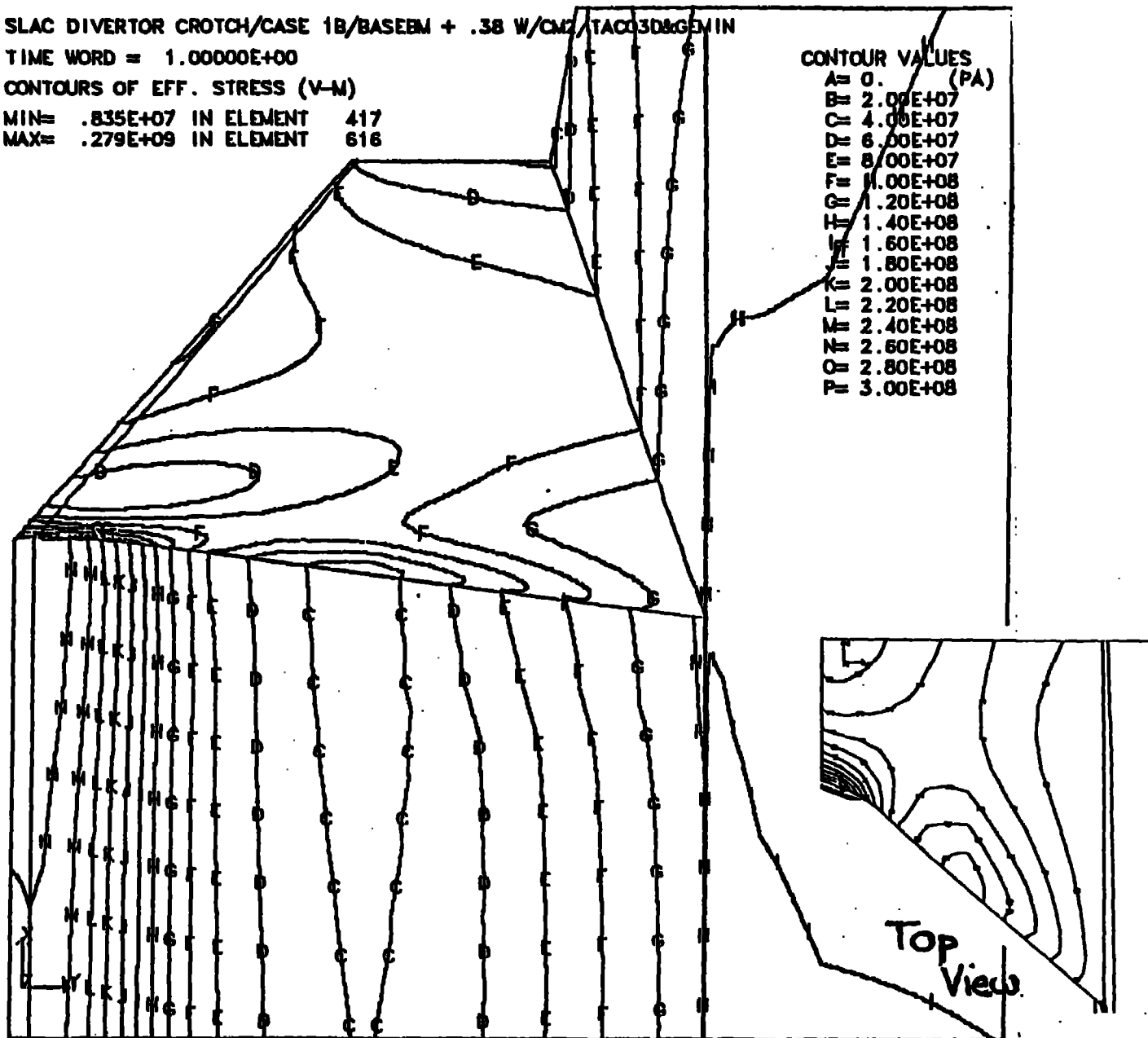N= 2.60E+08
O= 2.80E+08
P= 3.00E+08

Top View

Figure 28. Isobar plot (front view) of the modeled part for the base
geometry case (#1A) studying the effect of the heat
transfer coefficient, h=3.8 W/cm^2.

SLAC DIVERTOR CROTCH/CASE 1B/BASEBM + .38 W/CM2/TACO3D&GEMIN
TIME WORD = 1.00000E+00
CONTOURS OF EFF. STRESS (V-M)
MIN= .835E+07 IN ELEMENT 417
MAX= .279E+09 IN ELEMENT 616

CONTOUR VALUES
A= 0.   (PA)
B= 2.00E+07
C= 4.00E+07
D= 6.00E+07
E= 8.00E+07
F= 1.00E+08
G= 1.20E+08
H= 1.40E+08
I= 1.60E+08
J= 1.80E+08
K= 2.00E+08
L= 2.20E+08
M= 2.40E+08
N= 2.60E+08
O= 2.80E+08
P= 3.00E+08

Figure 29. Isobar plot (front view) of the modeled part for the base
geometry case (#1B) studying the effect of the heat
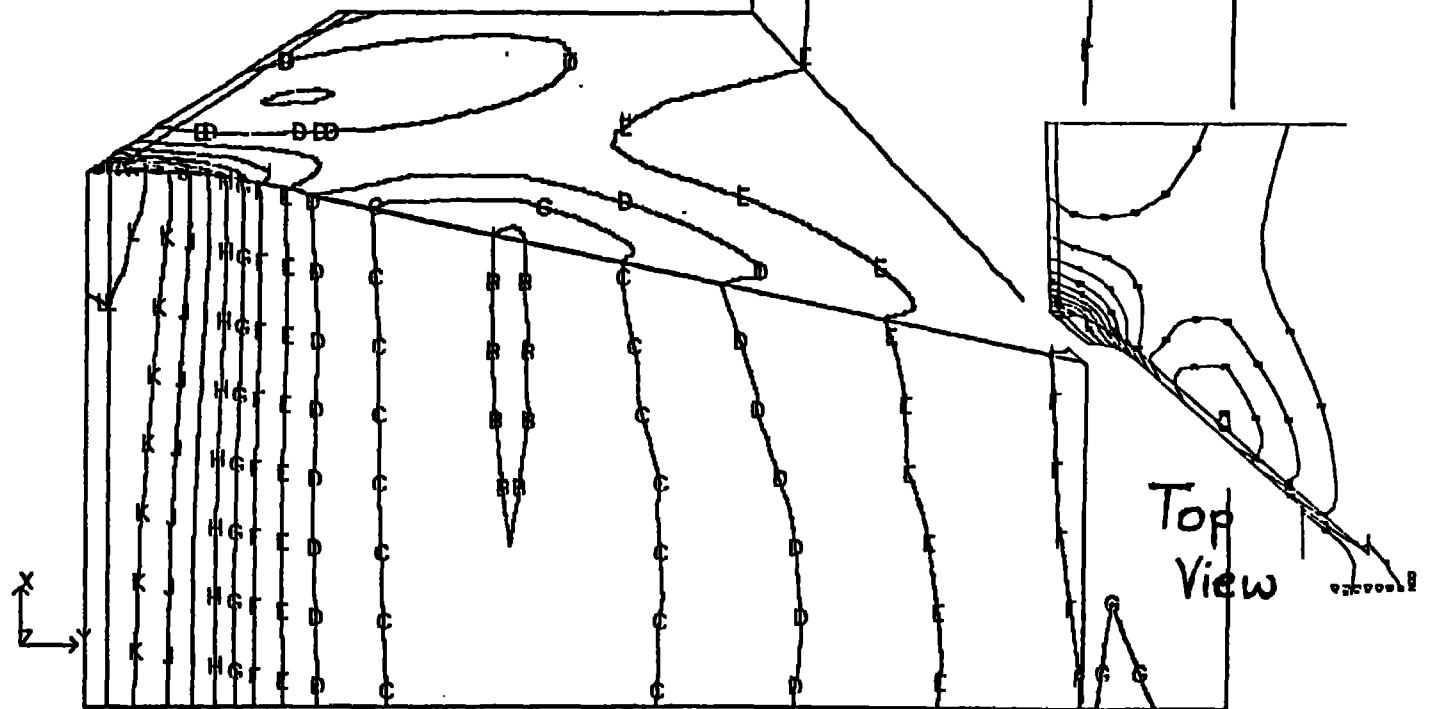transfer coefficient, h=0.38 W/cm^2.

Figure 30. Isobar plot (front view) of the modeled part for the base
geometry case (#1D) studying the effect of the heat
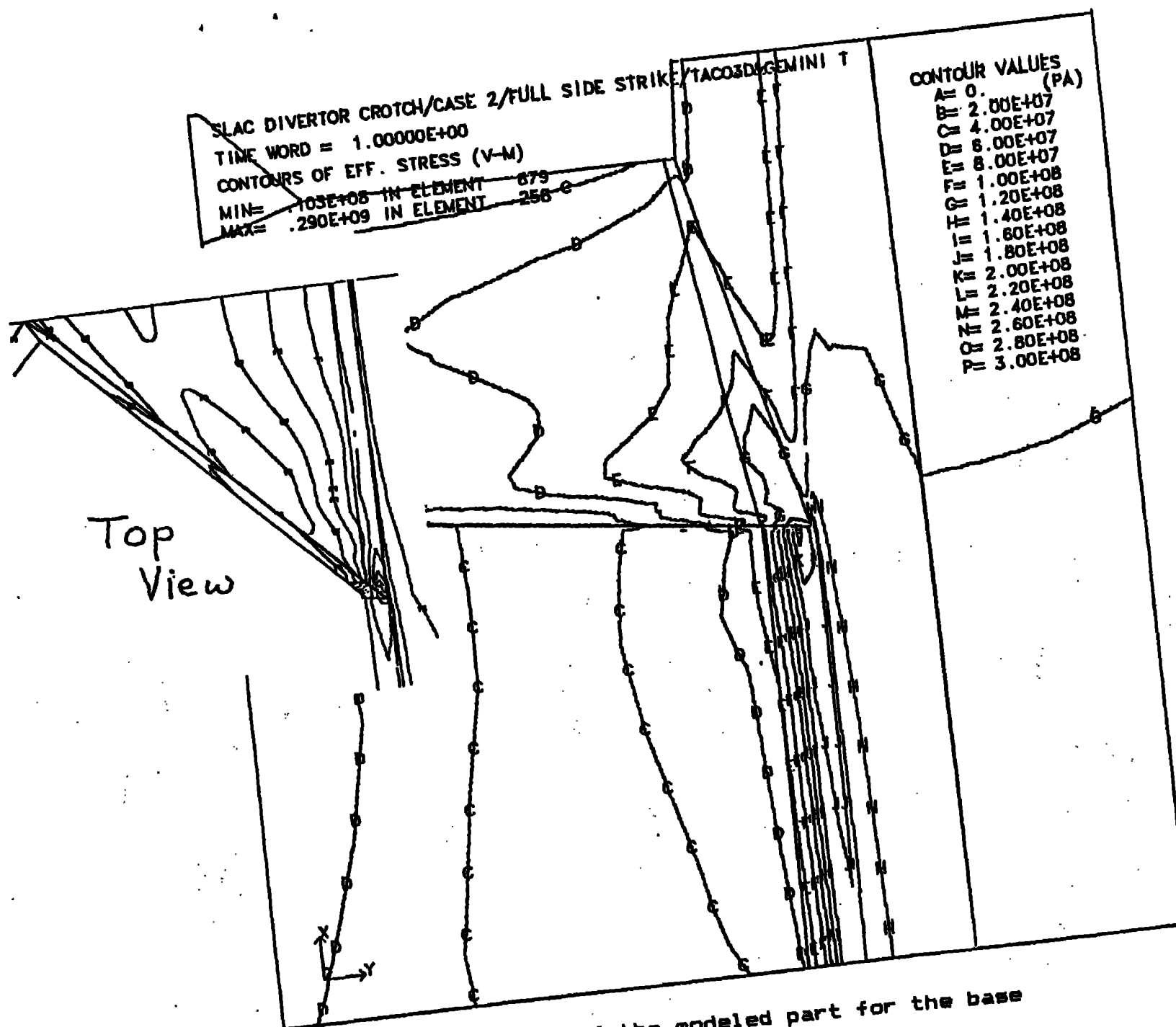transfer coefficient, h=1.9 W/cm^2.

Figure 31. Isobar plot (front view) of the modeled part for the base geometry case (#2) studying the effect of asymmetric h ting
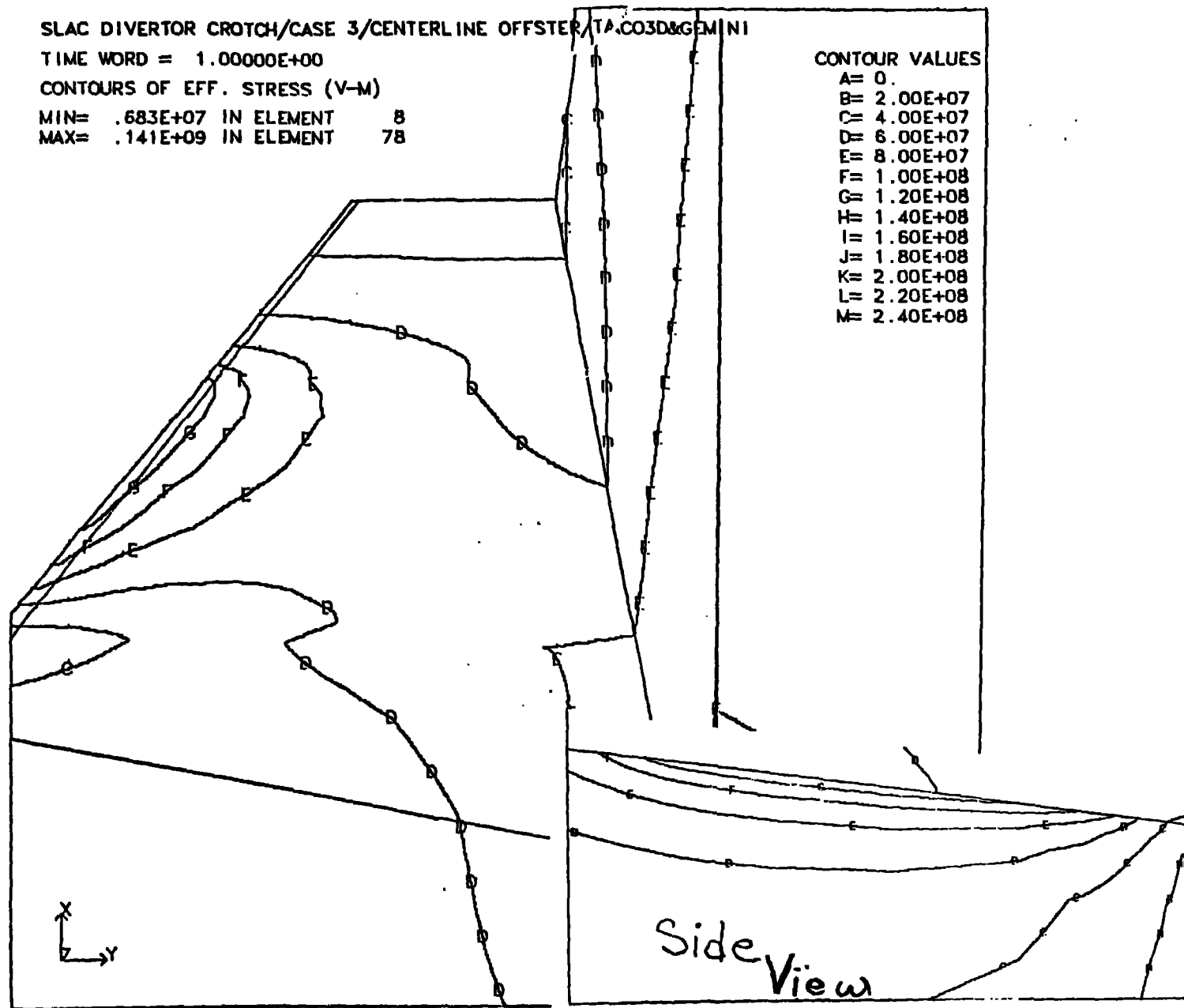
Figure 32. Isobar plot (front view) of the modeled part for the base geometry case (#3) studying the effect of unulator heating.

SLAC DIVERTOR CROTCH/CASE 4/LOWNOSE + 1.9 W/CM2/TACO3D&GEMINI

TIME WORD = 1.00000E+00

CONTOURS OF EFF. STRESS (V-M)

MIN= .120E+08 IN ELEMENT   657
MAX= .311E+09 IN ELEMENT   312

CONTOUR VALUES
A= 0.   (PA)
B= 2.00E+07
C= 4.00E+07
D= 6.00E+07
E= 8.00E+07
F= 1.00E+08
G= 1.20E+08
H= 1.40E+08
I= 1.60E+08
J= 1.80E+08
K= 2.00E+08
L= 2.20E+08
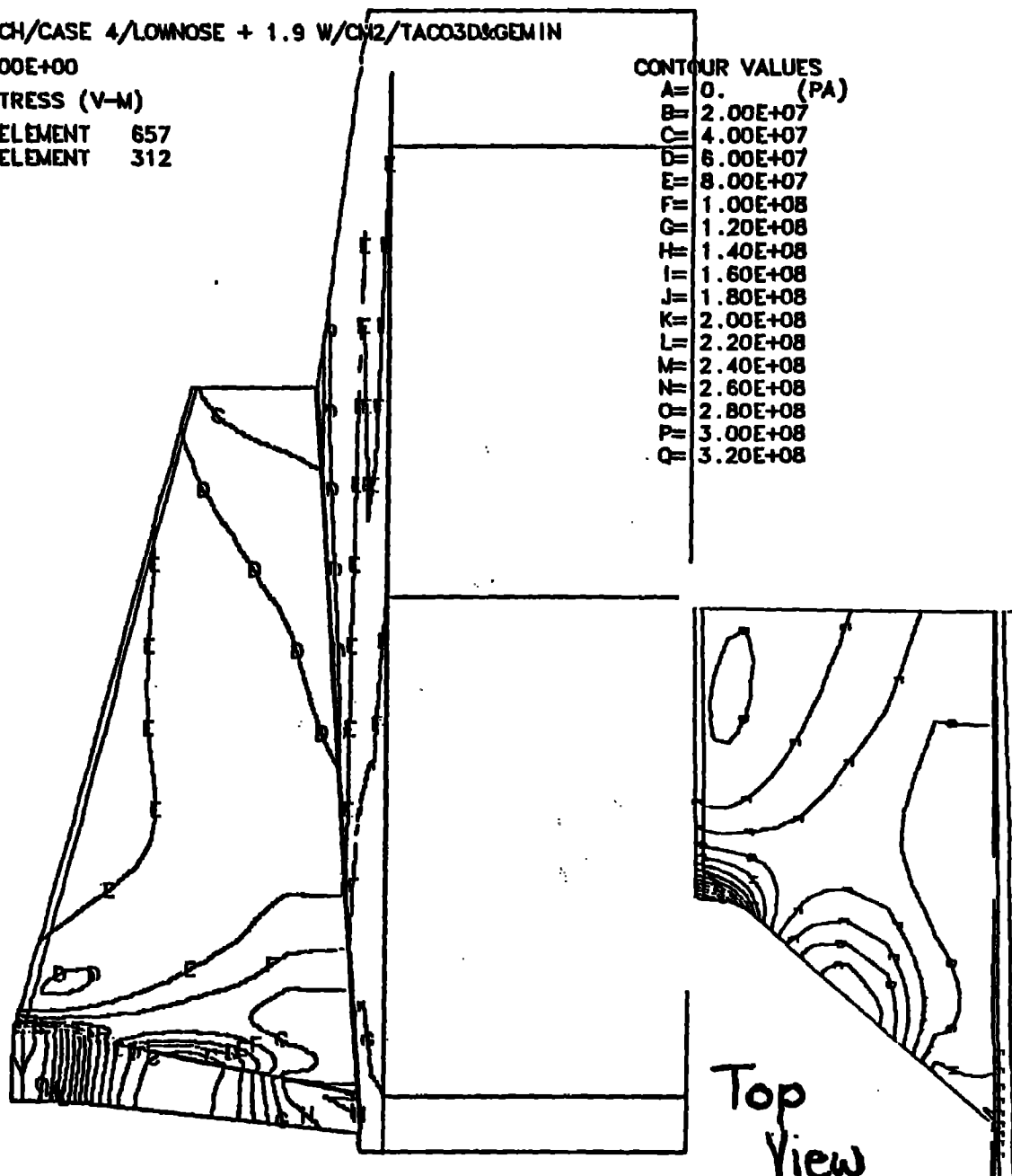M= 2.40E+08
N= 2.60E+08
O= 2.80E+08
P= 3.00E+08
Q= 3.20E+08

Top
View

Figure 33. Isobar plot (front view) of the modeled part for the low-
nose geometry case (#4) studying the effect of nose
height, (minimum nose height=1 mm).

SLAC DIVERTOR CROTCH/CASE 5/MIDNOSE + 1.9 W/CM2/TAC 3D&GEMIN

TIME WORD = 1.00000E+00

CONTOURS OF EFF. STRESS (V-M)

MIN= .481E+07 IN ELEMENT 670
MAX= .244E+09 IN ELEMENT 312

CONTOUR VALUES
A= 0.   (PA)
B= 2.00E+07
C= 4.00E+07
D= 6.00E+07
E= 8.00E+07
F= 1.00E+08
G= 1.20E+08
H= 1.40E+08
I= 1.60E+08
J= 1.80E+08
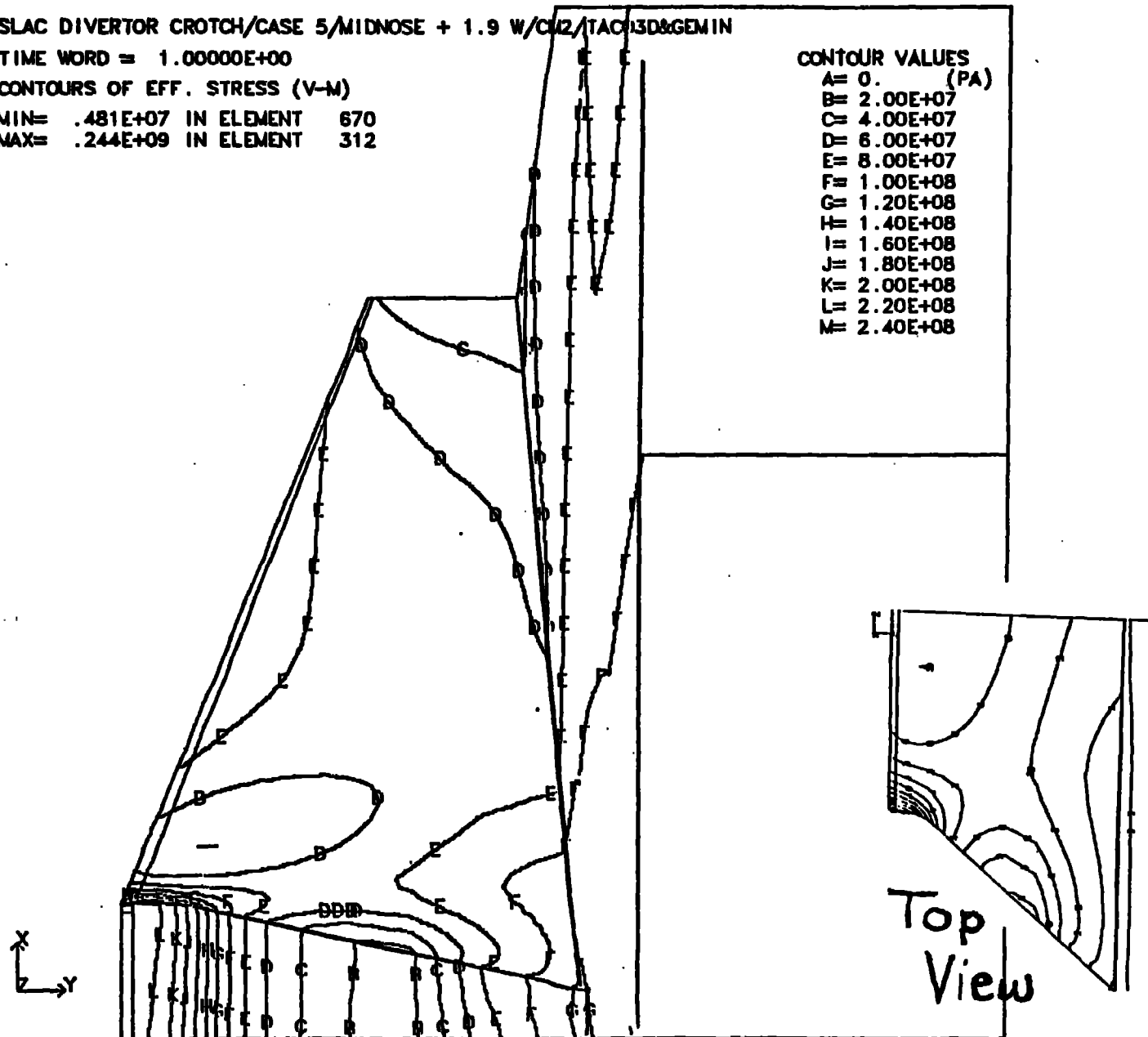K= 2.00E+08
L= 2.20E+08
M= 2.40E+08

Top
View

Figure 34. Isobar plot (front view) of the modeled part for the mid-
nose geometry (#5) case studying the effect of nose
height, (minimum nose height=6 mm).

APPENDIX A

ADDITIONAL FIGURES FROM ANALYSES OF DIVERTOR THERMAL STRESSES

Additional figures are
available in a three inch thick binder
from Richard Boyce (SLAC)
and Gary L. Johnson (LLNL)

APPENDIX B

MEMORANDUM ON POTENTIAL FOR CRACK GROWTH IN THE SLAC DIVERTOR CROTCH

00

May 31, 1985

MEMORANDUM — MTE 85-180

TO: G. L. Johnson

FROM: R. A. Riddle

SUBJECT: ASSESSMENT OF THE POTENTIAL FOR CRACK GROWTH IN THE
           SLAC DIVERTOR CROTCH

INTRODUCTION

This memo summarizes a brief analytical effort to assess the probability of crack growth in the 6061-T6 aluminum divertor crotch. The potential for crack growth arises from the exposure of the aluminum divertor crotch to a narrow (0.6 mm) beam of intense radiation. The beam of radiation causes localized heating in the aluminum.

The localized heating in turn creates temperature gradients which cause stresses in the divertor crotch due to differential thermal expansion. These thermally induced stresses exceed the yield strength of the material at their highest value, causing plastic deformation. This plastic deformation is the cause of residual stresses, which are stresses that remain in the material even after the temperature gradients are gone. These residual stresses commonly cause microcracking in aluminum, along the boundary which separates the regions of plastic and elastic deformation. Given the likelihood of microcracking, the question is to assess whether these microcracks may grow and cause structural failure of the divertor.

STRESS ANALYSIS

Using your results from a finite element analysis of the divertor, contours of the maximum principal stress were plotted (see the attached figures). Crack growth is expected in the direction of the largest maximum principal stress gradient, which direction would be normal to the contours of maximum principal stress at the points where the contours are most closely spaced.

Using the most simple fracture mechanics approach, the potential for crack growth was estimated using the equation

$$K_I = \sigma \sqrt{\pi a}$$

Where K_I is the applied stress intensity factor, σ is the far-field stress, assumed to be uniform, and "a" is the half-crack length. Crack growth occurs when, for a given crack length, the stress increases to the point where

$$K_I = K_{Ic}$$

where K_{Ic} is a material property termed the critical stress intensity factor. For 6061-T6 aluminum, K_{Ic} is assumed to be 29.7 MPa$\sqrt{m}$, and the yield stress is likewise 290 MPa (Handbook values, room temperature data, from Damage Tolerant Design Handbook, Metals and Ceramics Information Center, Battelle, Columbus, Ohio).

Although the stress field in this case is very different from the uniform stress field at infinity assumed in deriving the formula, the approach is to consider a very small flaw in the most highly stressed regions, and to see if such a flaw would propagate outward towards the channel wall, as if the crack were in a uniform stress field initially. Crack growth would be considered possible if the regions at high stress are large enough to accommodate flaws of the critical size. This should be a conservative approach.

To calculate these critical flaw sizes, the first formula is rearranged to give

$$a_{cr} = \left(\frac{K_{Ic}}{\sigma}\right)^2 \frac{1}{\pi}$$

For the far-field stress assumed to be at the room temperature yield strength, the critical crack size is 3.3 mm. For the far-field stress assumed to be 186.6 MPa (the stress contour value of the H fringe in the stress contour plots) the critical flaw size is 8.1 mm.

Since the total distance from the center of the divertor to the divertor wall is 10.5 mm, the regions of high stress are not sufficiently large to contain critical flaw sizes. Therefore, crack propagation from the regions high stress to divertor channel wall is not predicted.

A much more sophisticated analysis could be performed, but based upon these simple calculations, and noting how rapidly the maximum principal stress approaches very low values, crack growth in the divertor crotch which would cause a structural failure is not possible, given the current definition of the problem.

Robert A. Riddle
Materials Test & Evaluation Section
Engineering Sciences Division

RAR:MDM

SLAC DIVERTOR CROTCH/CASE 1D/BASEBM + 1.9 W/CM2/TACO3D&GEMIN

TIME WORD = 1.00000E+00

CONTOURS OF MAXIMUM PRINC STRESS

MIN= -.145E+08 IN ELEMENT   122
MAX= .236E+09 IN ELEMENT   616

CONTOUR VALUE.
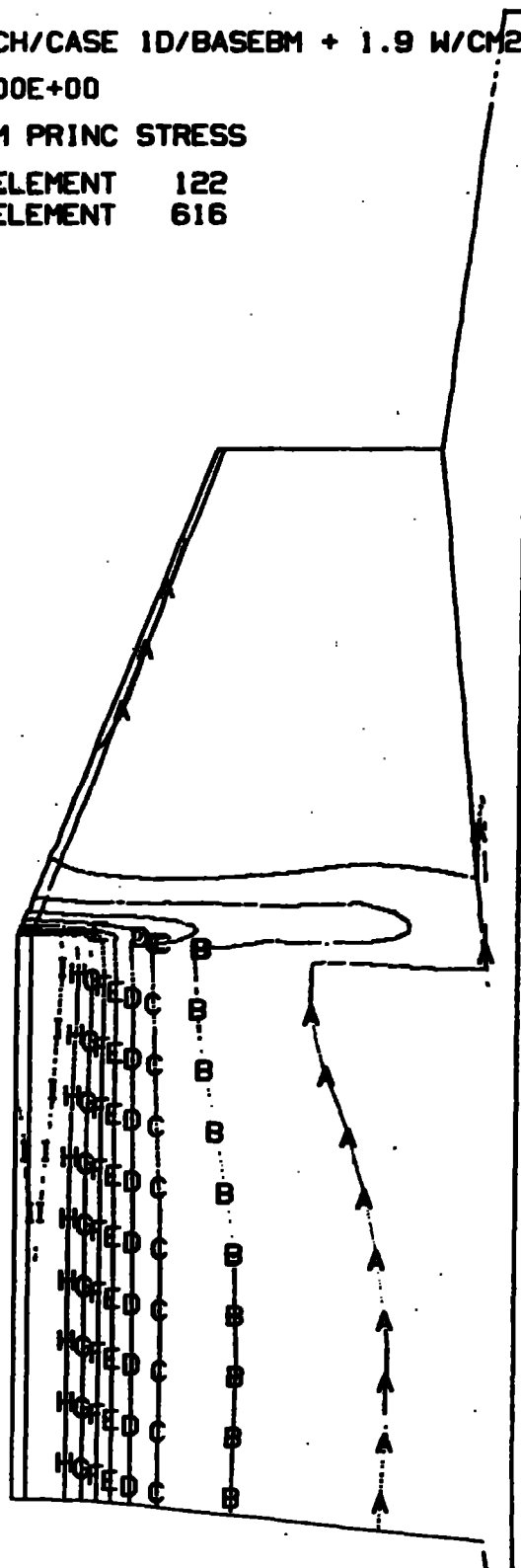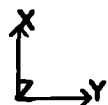A= 1.05E+07
B= 3.56E+07
C= 6.06E+07
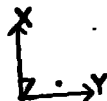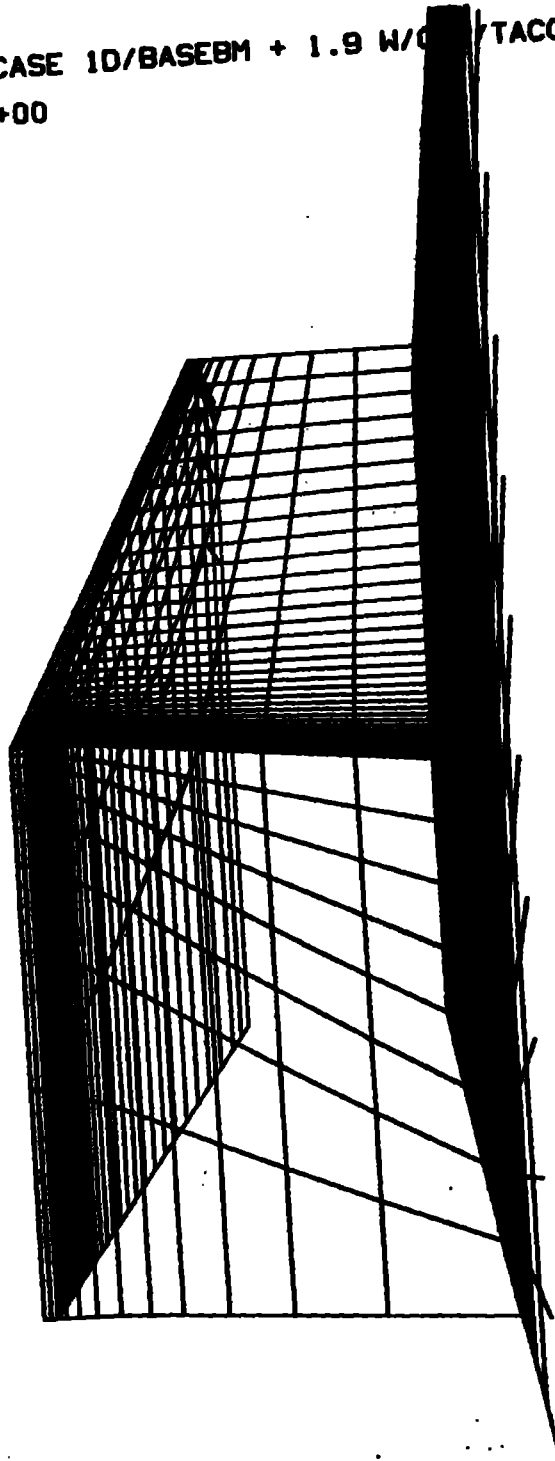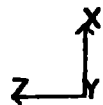D= 8.57E+07
E= 1.11E+08
F= 1.36E+08
G= 1.61E+08
H= 1.86E+08
I= 2.11E+08

SLAC DIVERTOR CROTCH/CASE 1D/BASEBM + 1.9 W/C   /TACO3D&GEMIN
TIME WORD =   1.00000E+00

X
Z Y

SLAC DIVERTOR CROTCH/CASE 1D/BASEBM + 1.9 W/CM2/TACO3D&GEMIN

TIME WORD = 1.00000E+00

CONTOURS OF MAXIMUM PRINC STRESS

MIN= -.145E+08 IN ELEMENT   122
MAX= .236E+09 IN ELEMENT   616

CONTOUR VALUES
A= 1.05E+07
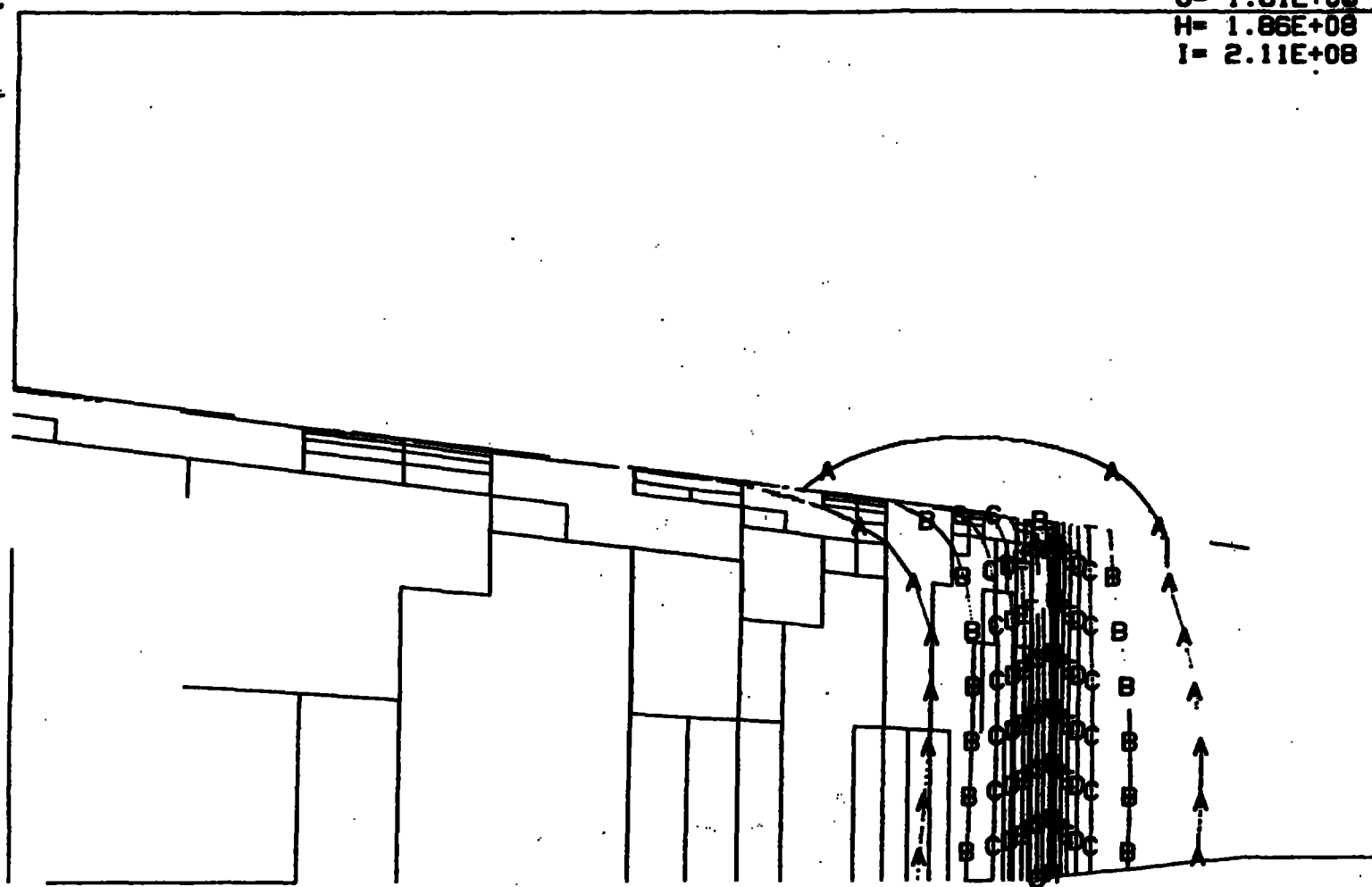B= 3.56E+07
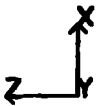C= 6.06E+07
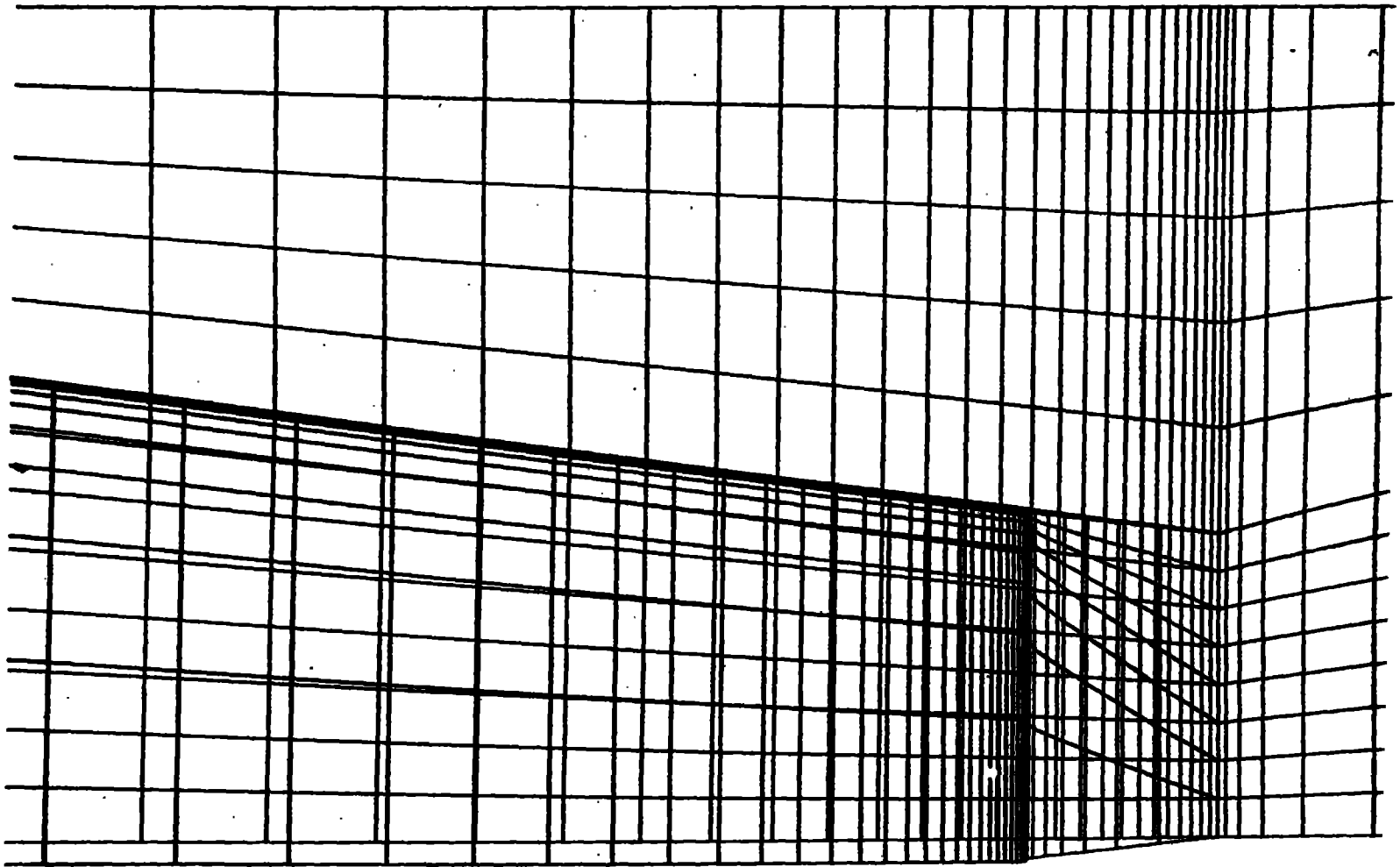D= 8.57E+07
E= 1.11E+08
F= 1.36E+08
G= 1.61E+08
H= 1.86E+08
I= 2.11E+08

X

Z   Y

SLAC DIVERTOR CROTCH/CASE 1D/BASEBM + 1.9 W/CM2/TACO3D&GEMIN

TIME WORD = 1.00000E+00

X

Z — Y

SLAC DIVERTOR CROTCH/CASE 1D/BASEBM + 1.9 W/CM2/TACO3D&GEMIN

TIME WORD = 1.00000E+00

CONTOURS OF MAXIMUM PRINC STRESS

MIN= -.145E+08 IN ELEMENT   122
MAX=   .236E+09 IN ELEMENT   616

CONTOUR VALUES
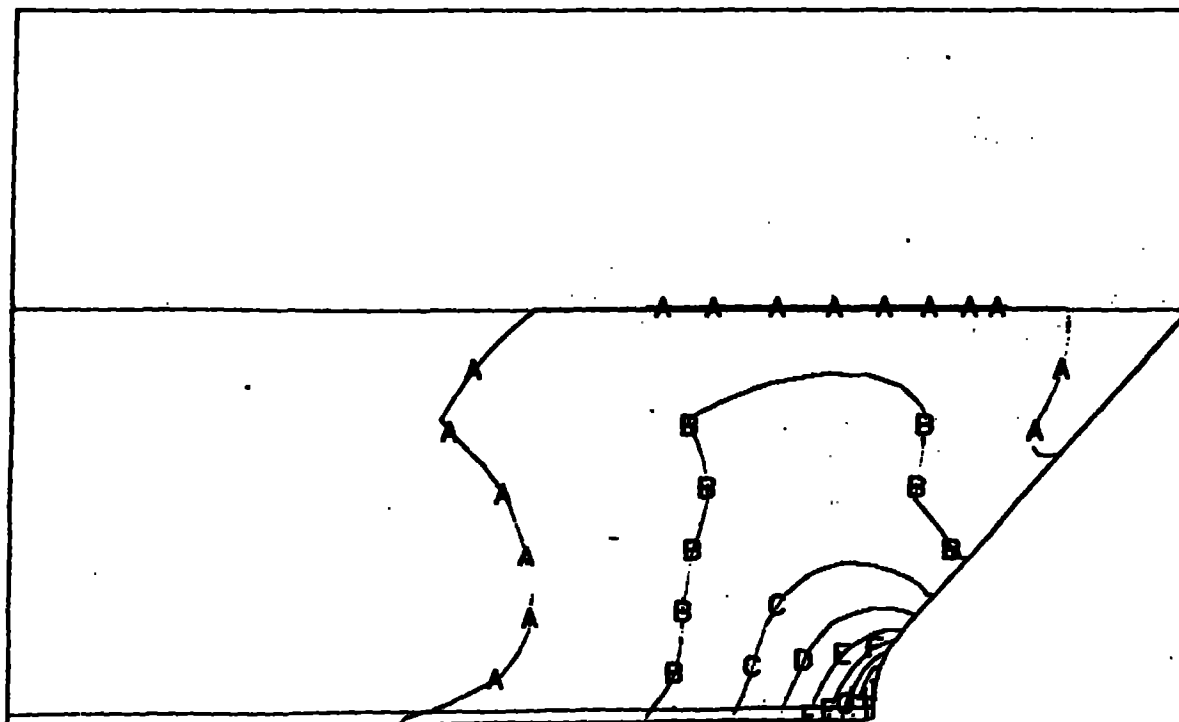A= 1.05E+07
B= 3.56E+07
C= 6.06E+07
D= 8.57E+07
E= 1.11E+08
F= 1.36E+08
G= 1.61E+08
H= 1.86E+08
I= 2.11E+08

SLAC DIVERTOR CROTCH/CASE 1D/BASEBM + 1.9 W/CM2/TACO3D&GEMIN
TIME WORD = 1.00000E+00